

Accepted Manuscript

Organometallic ruthenium(II)-arene complexes with triphenylphosphine amino acid bioconjugates: Synthesis, characterization and biological properties

Margareta Pernar, Zoran Kokan, Juran Kralj, Zoran Glasovac, Lidija-Marija Tumir, Ivo Piantanida, Domagoj Eljuga, Iztok Turel, Anamaria Brozovic, Srećko I. Kirin

PII: S0045-2068(18)30960-X
DOI: <https://doi.org/10.1016/j.bioorg.2019.03.048>
Reference: YBIOO 2874

To appear in: *Bioorganic Chemistry*

Received Date: 30 August 2018
Revised Date: 5 March 2019
Accepted Date: 15 March 2019

Please cite this article as: M. Pernar, Z. Kokan, J. Kralj, Z. Glasovac, L-M. Tumir, I. Piantanida, D. Eljuga, I. Turel, A. Brozovic, S.I. Kirin, Organometallic ruthenium(II)-arene complexes with triphenylphosphine amino acid bioconjugates: Synthesis, characterization and biological properties, *Bioorganic Chemistry* (2019), doi: <https://doi.org/10.1016/j.bioorg.2019.03.048>

This is a PDF file of an unedited manuscript that has been accepted for publication. As a service to our customers we are providing this early version of the manuscript. The manuscript will undergo copyediting, typesetting, and review of the resulting proof before it is published in its final form. Please note that during the production process errors may be discovered which could affect the content, and all legal disclaimers that apply to the journal pertain.



Organometallic ruthenium(II)-arene complexes with triphenylphosphine amino acid bioconjugates: Synthesis, characterization and biological properties

Margareta Pernar,^{a,#} Zoran Kokan,^{b,#} Juran Kralj,^a Zoran Glasovac,^c Lidija-Marija Tumir,^c Ivo Piantanida,^c Domagoj Eljuga,^d Iztok Turel,^e Anamaria Brozovic,^{a,*} Srećko I. Kirin,^{b,*}

^a Division of Molecular Biology, Ruđer Bošković Institute, Bijenička cesta 54, HR-10000 Zagreb, Croatia

^b Division of Materials Chemistry, Ruđer Bošković Institute, Bijenička cesta 54, HR-10000 Zagreb, Croatia

^c Division of Organic Chemistry and Biochemistry, Ruđer Bošković Institute, Bijenička cesta 54, HR-10000 Zagreb, Croatia

^d Department for Oncoplastic and Reconstructive Surgery, University Hospital for Tumors, University Clinical Hospital Centre Sisters of Mercy, HR-10000 Zagreb, Croatia

^e Faculty of Chemistry and Chemical Technology, University of Ljubljana, Večna pot 113, SLO-1000 Ljubljana, Slovenia

equal contribution

*corresponding authors

E-mail: Anamaria.Brozovic@irb.hr, Srecko.Kirin@irb.hr

Key words: Ruthenium; *p*-Cymene; Phosphine ligands; Cytotoxicity; Cell death

Abstract.

(*p*-Cymene)-ruthenium bioconjugates **ML** (**1**) and **ML**₂ (**2**), bearing phosphane ligands substituted with chiral or non-chiral amino acid esters, **L**, were synthesized and characterized by instrumental methods (NMR, CD, MS) and DFT calculations (using the wB97xD functional). Cytotoxic activity of complexes **1** and **2** was investigated by using human cervical carcinoma cell line (HeLa) and MTT assay. Four (**2**_{pG}, **2**_{pA}, **2**_{mG} and **2**_{mA}) out of ten synthesized ruthenium complexes showed significant toxicity, with IC₅₀ values of 5 to 30 μM. Evaluation of the potential biomolecular targets of bioconjugates **2** by UV-Vis, fluorescence and CD spectroscopy revealed no measurable interaction with DNA, but micromolar affinity for proteins. The cytotoxicity of bioconjugates **2** is in correlation with their BSA binding constants, i. e. bioconjugates with lower IC₅₀ values show higher binding affinities towards BSA. Compound **2**_{mG} with value of IC₅₀ 16 μM was selected for further biological characterization. The higher level of toxicity towards tumor compared to normal cell lines indicates its selective activity, important characteristic for potential medical use. It was detected **2**_{mG} caused increase of cells in the S phase of cell cycle and consequential decrease of cells in G₀/G₁ phase. Additionally, **2**_{mG} caused dose- and time-dependent increase of SubG₀/G₁ cell population, suggesting its ability to induce programmed cell death. Further investigation determined autophagy as the mode of cell death. The role of GSH in HeLa cells response to investigated organometallic ruthenium complexes was confirmed using specific regulators of GSH synthesis, buthionine sulfoximine and N-acetyl-cysteine. Pre-treatment of cells with ethacrynic acid and probenecid emphasized the role of GSH in detoxification of **2**_{mG} compound. The amount of total ruthenium accumulation in the cell did not correlate with toxicity of **2**_{pG}, **2**_{pA}, **2**_{mG} and **2**_{mA}, suggesting structure dependent differences in either cell uptake or kinetics of ruthenium complexes detoxification. We speculate that ruthenium complexes bind protein-based biomolecules further triggering cell death. Based on the gained knowledge, the synthesis and development of more tumor-specific ruthenium-based complexes as potential anticancer drugs can be expected.

Introduction.

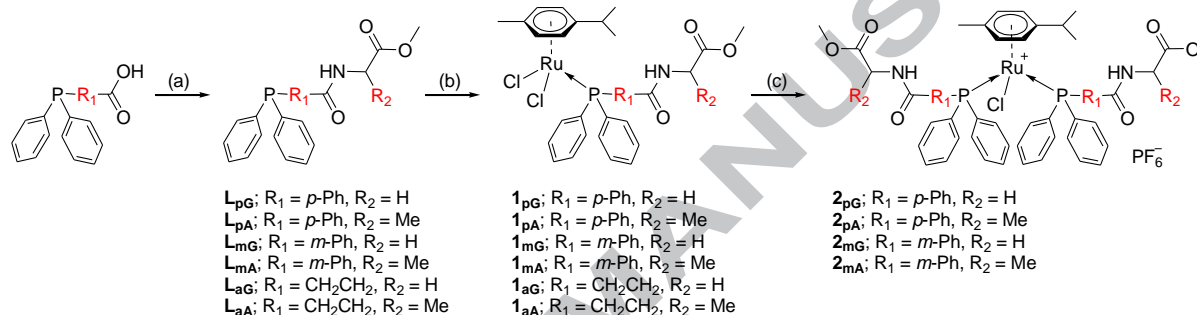
Besides the importance of ruthenium (Ru) complexes in catalysis, a major area of research interest is their medical implementation. Although frequently in use, the platinum-based compounds, as an example of prominent inorganic anticancer complexes, have several limitations such as development of drug resistance, side effects and ineffectiveness towards certain tumors (Brozovic and Osmak 2007, Galluzzi et al 2012). In recent years, ruthenium complexes displayed some superior properties over platinum-based drugs (Bergamo and Sava 2015, Vajs et al 2015). Despite the fact that none of the ruthenium complexes is still in clinical use as anticancer drug, prominent representatives like NAMI-A, KP1019, RAPTA and TLD1433 scored success in *in vitro* and *in vivo* studies, prompting ruthenium complexes to rapidly become a major area in anticancer drug innovation (Bergamo and Sava 2015, Blunden et al 2014, Domotor et al 2013, Meier-Menches et al 2018, Sersen et al 2015). The wide variety of ruthenium anticancer complexes studied in recent years includes derivatives with amino acids (Rathgeb et al 2014, Scrase et al 2015) and derivatives with triphenylphosphines (Biancalana et al 2017, Chaplin et al 2007, Martinez et al 2017, Millan 2019).

Nowadays, a number of anticancer metal complexes are in the developmental phase and are mostly designed to mimic broadly used cisplatin, known to target DNA. Aside from the DNA damage, cisplatin is able to induce reactive oxygen species (ROS) and endoplasmic reticulum stress, as well as bind to peptides and proteins (Brozovic et al 2010). Similarly, recent studies examining ruthenium anticancer compounds revealed that DNA is not always the primary target and that these compounds bind proteins stronger than to DNA (Gasser et al 2011, Novakova et al 2005, Ravera et al 2004, Scolaro et al 2007). Based on those findings, different modes of ruthenium compounds cytotoxic actions occur, although the exact mechanism is still not known. What is known is the fact that cancer cells are generally growing and multiplying much faster than normal healthy cells, creating a reductive environment due to the raised metabolic rate, higher levels of glutathione (GSH) and a lower pH (Antonarakis and Emadi 2010). Moreover, it was shown that ruthenium complexes interact with GSH (Wang et al 2005) and GSH-associated enzymes (Lin et al 2013), implying the role of the GSH in cells' defense against toxic damage (Sommer et al 2014).

Amino acid bioconjugates of triphenylphosphanes are well known ligands for the coordination of transition metals. We have studied the self-assembly and biological properties of their palladium and platinum complexes (Kokan et al 2017, Kokan et al 2018) and successfully used them as monodentate ligands in rhodium catalyzed asymmetric hydrogenations (Kokan and Kirin 2012, Kokan and Kirin 2013, Kokan et al 2014, Opačak et al 2019). A major feature of those metal complexes is the formation of chiral secondary structures responsible for chiral induction in the catalytic cycle. Herein, we explore the synthesis and characterization of (*p*-cymene)ruthenium complexes **1** and **2**, bearing phosphane ligands **L** with chiral or non-chiral amino acid esters. The spacer between the phosphorus and the amino acid was varied in order to investigate hydrogen-bonding propensity of the amino acid substituents. Structural and biological properties of the prepared complexes will be reported.

Results and discussion.

Synthesis and characterization. The chemical synthesis of the presented organometallic complexes was performed in solution in several steps, **Scheme 1**. First, the free carboxylic acid of the phosphine precursors $\text{Ph}_2\text{P-}p\text{C}_6\text{H}_4\text{-CO}_2\text{H}$, $\text{Ph}_2\text{P-}m\text{C}_6\text{H}_4\text{-CO}_2\text{H}$ or $\text{Ph}_2\text{P-C}_2\text{H}_4\text{-CO}_2\text{H}$ was reacted with N-protected amino acid methyl esters of achiral glycine or chiral L-alanine in standard conditions for amide bond formation to yield amino acid triphenylphosphine ligand bioconjugates **L**, **Scheme 1**. In the second step, ligand bioconjugates **L** and ruthenium precursor $[(p\text{Cym})\text{RuCl}]_2\text{Cl}_2$ were combined to give mono-complexes **1**, with 1:1 metal to ligand stoichiometry, general formula $[(p\text{Cym})\text{RuLCl}_2]$. Finally, in the last synthetic step, mono-complexes react with one additional equivalent of the corresponding ligand and the bis-complexes **2** were obtained, $[(p\text{Cym})\text{RuL}_2\text{Cl}](\text{PF}_6)$, with 1:2 metal to ligand stoichiometry. In total, six ligands and ten complexes were prepared. Unfortunately, complexes **2_{aG}** and **2_{aA}**, although clearly present in the crude reaction mixture, could not be isolated pure enough for further studies.



Scheme 1, experimental conditions: (a) TBTU/HOBT/DIPEA/DCM, amino acid ester hydrochloride, RT, 15 h; (b) Di- μ -chlorobis[*p*-cymene]chlororuthenium(II)/DCM, RT, 2 h; (c) 1. $\text{NH}_4\text{PF}_6/\text{AcCN}$, reflux, 45 min, 2. **L**/DCM, RT, 15 h.

The ligands and complexes were characterized by NMR (^1H , ^{13}C and ^{31}P), CD spectroscopy and MALDI high resolution mass spectrometry. In particular, the ^{31}P shifts of the phosphine moiety in ligands **L** ($\delta_{\text{P}} \approx -5$ ppm), mono- and bis-complexes **ML** ($\delta_{\text{P}} \approx 25$ ppm) and **ML₂** ($\delta_{\text{P}} \approx 22$ ppm) clearly indicate binding to the ruthenium metal in the different stoichiometry. The NH proton chemical shifts for **L**, **ML** and **ML₂** indicate only weak intramolecular hydrogen bonding in **ML₂** complexes ($\delta_{\text{NH}} < 7.15$ ppm in CDCl_3). It is interesting to note that the C2 proton in **1_{mG}** and **1_{mA}** are unexpectedly highly deshielded ($\delta_{\text{H}} \approx 8.9$ ppm). Selected characteristic NMR data are collected in Table S1.

Computational study. Relative Gibbs energies of the ruthenium complexes were calculated using wB97xD density functional approach, **Table S2**. This functional was confirmed as very good in rationalizing enantioselectivity in a rhodium catalyzed hydrogenation reaction and in predicting geometries of organic molecules and transition metal complexes including ruthenium complexes (Gridnev and Imamoto 2015, Minenkov et al 2012). Further, this functional is the recommended method when weak interactions like π - π interactions are expected (Qi et al 2016). Four complex cations with 2:1 ligand to metal stoichiometry, **2_{mG}**, **2_{pG}**, **2_{mA}** and **2_{pA}**, were chosen for the calculations, containing *meta*- or *para*-substituted triphenylphosphine ligand conjugated with glycine or alanine methyl ester, respectively and several conformations were considered for each of the cations. Relative energies of all optimized conformers of the ruthenium complex cations are collected in **Table S2** (supplement). In addition, Cartesian coordinates of all computed structures are available as a single separate text file, for visualization and analysis.

All calculated conformations contain aromatic stacking interactions ($\pi - \pi$ stacking) between two different triphenylphosphine moieties, but with a different number of intramolecular hydrogen bonds between the ligands. In the case of 2_{mG} , a representative conformation was generated with the aid of NMR experiments. NOESY experiment suggests position of amide protons in close proximity to the C2 and C4 atoms of the stacked phenylene subunit and also to the cymene ligand. This information indicates a "syn-Phe" orientation of two 1,3-phenylene subunits forming a curved shape of the complex. Chloride ligand is directed outward the structure of complex.

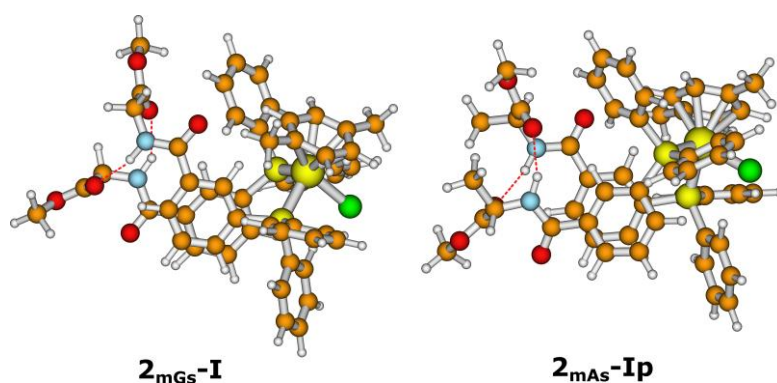


Figure 1. Optimized structures of 2_{mGs-I} and 2_{mAs-Ip} .

In context of intramolecular H-bonds between the ligands, both "syn-Phe" (2_{mGs}) and "anti-Phe" (2_{mGa}) conformers can exist in a Herrick (I) or van Staveren (II) arrangement. Several conformers satisfying a "syn-Phe" arrangement were optimized and the lowest energy one shows a Herrick-type of hydrogen bonding motif (2_{mGs-I}). During our attempts to optimize 2_{mGs-II} conformer, reorganization of the hydrogen bonds occurred and the optimization ended up in "semi-Herrick" structure (2_{mGs-Ib}) with only one NH-OCOME hydrogen bond. We were able to optimize van Staveren conformer 2_{mGs-II} only with cymene ligand moved away from the stacked phenylene fragment. However, this structure strongly disagrees with the NOESY data and it is not likely present in solution. According to DFT calculations, 2_{mGs-I} is more stable than 2_{mGa-I} , 2_{mGs-II} and 2_{mGa-II} by 11, 13 and 33 kJ mol^{-1} , respectively. The lowest stability of conformer 2_{mGa-II} , with only one hydrogen bond, is in good accordance with our previous results on ferrocene amino acids (Kirin et al 2006). These results additionally support the structural indications obtained by NOESY experiment.

In the case of 2_{pG} , only one $\pi - \pi$ stacking motif with either Herrick or van Staveren hydrogen bonding scheme (2_{pG-I} and 2_{pG-II} , respectively) is possible. The calculations indicate the somewhat lower energy for 2_{pG-I} than for 2_{pG-II} conformers (by ca 6 kJ mol^{-1} , **Table S2**). Inspection of the geometrical parameters reveals significantly longer hydrogen bonds in 2_{pG-II} than in 2_{pG-I} (HB, above 2.0 Å vs. 1.919 Å) indicating origin of the energy difference.

The analogous conformers were also identified for the chiral L-alanine derivatives 2_{mAs} , 2_{mAA} and 2_{pA} . Only L-alanine derivatives were used for the calculations, to allow comparison with compounds experimentally prepared herein. The starting structures were generated from the glycine-based conformations by replacement of one C_{α} -proton with methyl group. Again, the most stable structure is characterized by "syn-Phe" arrangement of the stacked phenylene subunit with Herrick motif of hydrogen bonding (2_{mAs-Ip}) with P-type of helical chirality. This result confirms preferred "syn-Phe" arrangement in both aminoacid bioconjugates.

According to calculations, conformer **2_{mAs}-Ip** is more stable than **2_{mAs}-Im** and **2_{mAa}-Im**, by 20 and 18 kJ mol⁻¹, respectively. Calculated lower stability of M- helical isomers of **2_{mAs}-Im** with respect to its P- diastereomer is ascribed to the arrangement of two methyl groups of alanine fragments. More stable structure (P-helical isomer) has these two methyl groups relatively close to each other ($d = 4.088 \text{ \AA}$). Although one could expect pronounced sterical repulsion, this is apparently not the case. It is somewhat surprising that **2_{mAs}-Iip** lies only 8 kJ mol⁻¹ above **2_{mAs}-Ip** and it is more stable than **2_{mAa}-Im** in spite of reduced number of hydrogen bonds. The geometry of **2_{mAs}-Iip** is similar to **2_{mGs}-II** and, if we assume similar conformation of glycine and alanine derivatives, its presence in the solution is unlikely.

Finally, we shall briefly comment the structure of **2_{pA}** complex. The lowest Gibbs energy was obtained for the Herrick-type complex **2_{pA}-I** and it is more stable than **2_{pA}-II** by ca 11 kJ mol⁻¹. Relative stabilities of two diastereomers (defined by P- and M- helicity) in comparison to the isomer **2_{pA}-II** follows the same trend as for **2_{mAs}-I** derivative, P-helicity with the distance between the alanine methyl groups of 4.060 Å is preferred over the M- isomer by 19 kJ mol⁻¹. The latter is even less stable than **2_{pA}-II** by 5 kJ mol⁻¹.

Cytotoxicity. The cytotoxicity of ligands **L**, as well as their **ML** and **ML₂** ruthenium complexes, was examined by MTT assay; ruthenium precursor di- μ -chlorobis[(*p*-cymene)chloro-ruthenium(II)] was included for comparison. For this purpose, the well-known human cervical carcinoma cell line was used (HeLa), attested for screening of new compounds (Brozovic et al 2014, Cimboraz-Zovko et al 2011). The IC₅₀ value (the cytotoxicity of the compound expressed as the dose that reduced the survival of cells in 72 h MTT assay to 50% of the value obtained for control cells) was above 33.3 μM for all ligands **L** and mono-ligand ruthenium complexes **ML** (**Table S3**). The ruthenium precursor was not toxic for the cells (also **Table S3**). However, the IC₅₀ for bis-ligand ruthenium complexes **2_{pG}**, **2_{pA}**, **2_{mG}** and **2_{mA}** was 5–30 μM, making them interesting for further examination as potential antitumor compounds (**Table 1**). The compound **2_{pG}** was the least toxic and the **2_{mA}** was the most toxic one. In order to avoid the solvent's toxicity, concentrations above 33.3 μM were not used. In that way, the highest concentration of the solvent in the well was under 0.5 %, which is not toxic for the HeLa cells.

Table 1. The cytotoxic activity of the compounds towards the HeLa cells (IC₅₀ μM ± SD), after 72 h incubation. The cytotoxicity was measured by MTT assay. The experiments were repeated at least three times. Cp. = Compound.

Cp.	IC ₅₀ ± SD (μM)
2_{pG}	30±3.2
2_{pA}	15±3.7
2_{mG}	16±2.5
2_{mA}	5±2.7

The IC₅₀ values of 5 to 30 μM measured in HeLa cells for **ML₂** complexes presented herein were similar to the value obtained under same experimental conditions for broadly used chemotherapeutic, cisplatin (Stojanovic et al 2013). Moreover, our results for additional tumor cell lines investigated are similar to the values previously obtained for breast carcinoma (MDA-MB-231) cells, treated with ruthenium complexes substituted with amino acid. The authors concluded that the amino acids do not significantly affect the activity of the

complexes, but existence of the methyl groups in diamine increase their biological activity (Dos Santos et al 2016). The presence of triphenylphosphine group seems to increment the antitumor properties of Ru complexes through intercalation in the DNA of the human acute promyelocytic leukemia (HL60) cells with IC_{50} value 5.2 μ M (Saez et al 2014).

One of the criterions necessary for a newly synthesized complex to be considered as a potential antitumor compound is low toxicity for normal cells and non-selective toxicity for different tumor cell lines. With the purpose to test this criterion, for further experiments we decided to use **2_{mG}**, due to its medium value of toxicity within the studied series of compounds. In order to examine the toxic capacity of **2_{mG}** on different types of human tumor cells, the laryngeal carcinoma (HEp2), lung carcinoma (H460) and MDA-MB-231 cells were used. The collected data showed that **2_{mG}** is similarly toxic to all examined cancer cell lines (Table 2). However, the IC_{50} of **2_{mG}** for normal human cell line, keratinocytes, was far above the toxicity measured for all examined compounds; the same result was obtained for human fibroblasts (Table 2).

Table 2. The cytotoxic activity of the **2_{mG} towards different tumor and two normal cell lines (IC_{50} μ M \pm SD), after 72 h incubation.** The cytotoxicity was measured by MTT assay. The experiments were repeated at least three times. Cp. Compound.

Cp.	HEp2	H460	HeLa	MDA-MB-231	keratinocyte	fibroblast
2_{mG}	14 \pm 4.7	15 \pm 0.6	16 \pm 2.5	12.3 \pm 0.9	>33.3	>33.3

Potential biomacromolecule target evaluation. For the small bioactive molecules, determination of the main target within the living cell is a quite challenging and time-consuming task, particularly for the structures presented herein, that contain DNA-targeting and protein-targeting features. In general, condensed aryl-Ru complexes are well known DNA binders (Gasser et al 2011); however, here presented structures do not contain condensed arenes necessary for DNA intercalation, nor several positive charges which could interact with DNA-backbone. Nevertheless, attached amino acid residues could form several H-bonds within DNA minor groove. On the other side, general spherical shape of the studied molecules is characterized by high hydrophobicity and thus could be nicely accommodated within hydrophobic pockets of well-known carrier proteins like serum albumins, within which amino acid residues from the studied small molecules could additionally contribute to the protein-substrate complex formation by H-bonding.

To facilitate the planning and the analysis of demanding cellular experiments in respect of the main target choice, we studied interactions of several Ru-complexes with model DNA (calf thymus, *ct*-DNA) and model protein: serum albumin (BSA), as the most abundant protein in blood plasma, that is responsible for the transport of many small molecules (among which are drugs and probes) (Otagiri et al 2016, Peters et al 1995). Experiments were performed in simple, well-defined conditions in cuvettes, at biologically relevant conditions (buffered pH 7) containing only studied Ru-complex (micromolar concentration) and biomacromolecule (*ct*-DNA or BSA).

The studied Ru-complexes did not stabilize *ct*-DNA against thermal denaturation nor changed the DNA CD spectrum, thus showing no measurable interaction (**Figure S4**). However, addition of Ru-complexes induced measurable changes in the BSA CD spectrum at

240 – 290 nm (**Figure S5**), suggesting structural change in the protein chiral conformation; non-linear dependence of the CD change agreed well with a non-covalent binding event.

Furthermore, the intrinsic fluorescence of BSA significantly quenched upon Ru-complex addition. Multivariate analysis of the fluorimetric data by Specfit program (Gampp et al 1985, Maeder and Zuberbuhler 1990) revealed formation of 1:1 stoichiometry Ru-complex/BSA complex with micromolar affinity (**Figures S6-S9**). Intriguingly, non-linear dependence of the BSA CD spectrum changes at 260 nm (**Figures S6-S9, Table 3**) also supported similar binding affinity. Thus, results obtained suggest that the observed cytotoxic activity of compounds is not related to any interactions of complexes with the cellular DNA, but more likely with the protein target.

Table 3. Stability constants ($\log K_s$)^a and spectroscopic properties (ΔI)^b of the complexes that ruthenium(II)-arene compounds formed with BSA protein, calculated according to the fluorimetric titrations (Na-cacodylate buffer, $c = 0.05 \text{ mol dm}^{-3}$, $\text{pH} = 7.0$; $\lambda_{\text{exc}} = 300 \text{ nm}$; $\lambda_{\text{em}} = 320\text{-}450 \text{ nm}$, $c(\text{BSA}) = 5 \times 10^{-7} \text{ mol dm}^{-3}$).

Cp.	ΔI^b	$\log K_s^a$
2_{pG}	-95%	5.08±0.07
2_{pA}	-48%	5.99±0.07
2_{mG}	-57%	5.84±0.05
2_{mA}	-34%	6.50±0.09

^a Processing of titration data by Specfit program (Gampp et al 1985, Maeder and Zuberbuhler 1990) gave best fit for 1:1 stoichiometry; for all titrations concentration range corresponded to ca. 20-80% complexation.

^b Changes in fluorescence of BSA induced by complex formation ($\Delta I = (I_{\text{lim}} - I_0) \times 100 / I_0$); where I_0 was calculated emission intensity of free compound and I_{lim} was emission intensity of a complex calculated by Specfit program.

A similar protein binding affinity was observed previously for RAPTA-C, the Ru containing antimetastatic agent, that accumulates at specific histone site on the nucleosome core. It seems that changing the ethylenediamine ligand of $[\text{Ru-cymene-Cl}]^+$ to phosphadamantane (+Cl) switches the adduct formation profile from primary targeting the DNA to targeting the proteins associated with chromatin (Adhireksan et al 2014).

Interestingly, strong correlation between the cytotoxic activity of compounds towards HeLa cells (**Table 1**) and the stability constants of compound-BSA complexes (**Table 3**) was observed. Specifically, compound **2_{mA}** showed both the highest cytotoxic activity and the highest affinity for BSA constant, while **2_{pG}** showed the lowest cytotoxicity and the lowest stability constant toward BSA among examined compounds. This correlation additionally supported protein as one of the main biological targets for ruthenium complexes in this study.

Cell cycle. Further, we were interested to investigate the mechanism of toxicity of bis-ligand ruthenium complexes and for this purpose we treated HeLa cells with one of them; 16 μM **2_{mG}** during 24-72 h. Upon flow cytometric analysis it was shown that **2_{mG}** caused a slight time-dependent increase of cells in S phase of the cell cycle that is more visible in dose-response of cells to **2_{mG}** treatment, along with consequential decrease of cells in G₀/G₁ phase (**Figure 2A**). This was accompanied by the increase of the cells present in the SubG₀/G₁

fraction, which represent the population of dead cells. The increase of the SubG0/G1 cell fraction was confirmed by the treatment of HeLa cells during 72 h with different concentrations of 2_{mG} (Figure 2B). Deconvolution algorithm (Watson pragmatic) was used for cell cycle data analysis. The results were confirmed by time- and dose-dependent cell cycle analysis upon treatment of HEp2 cells with 2_{mG} , where increase of the cell amount in S phase of the cell cycle is more visible compared to the HeLa cells due to their higher sensitivity to 2_{mG} (Figure S11).

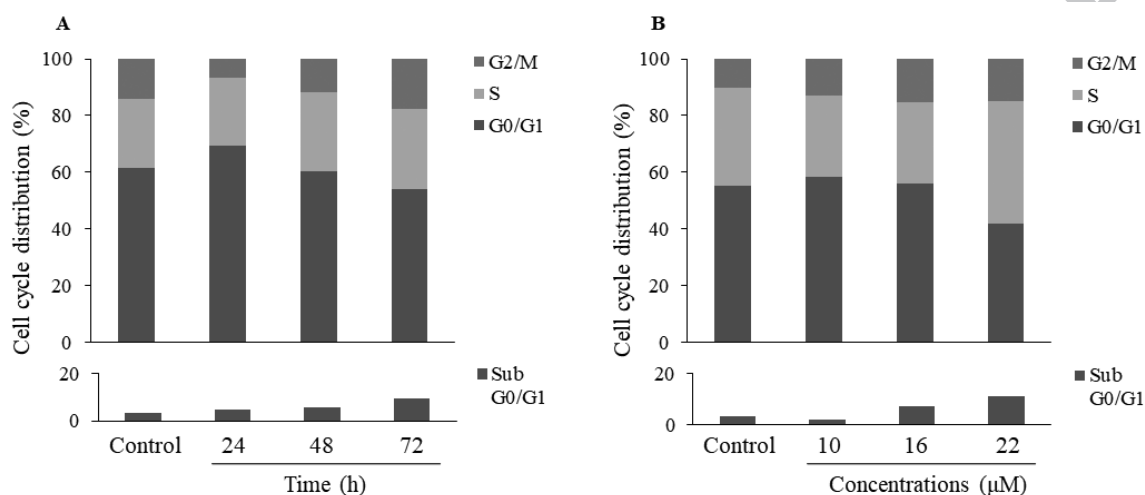


Figure 2. 2_{mG} compound induces increase of HeLa cells in S phase and consequential decrease of cells in G0/G1 phase of the cell cycle, and an increase of SubG0/G1 cell population. Cells were treated either with 16 μM 2_{mG} during 24-72 h (A) or with different concentrations of 2_{mG} during 72 h (B). The data of one from three performed experiments are shown.

Cell death. Necrosis and apoptosis are two major types of cell death. Inappropriate regulation of both processes can result in several diseases, including cancer (Nikoletopoulou et al 2013). With the purpose to distinguish between necrotic and apoptotic cell death, HeLa cells were treated with different concentrations of 2_{mG} during 24-72 h and then stained with Annexin V-FITC and propidium iodide (PI). As shown in Figure 3, the percentage of PI negative (-)/Annexin V-FITC positive (+) and PI+/Annexin V-FITC+ cells increased with the time (Figure 3A) as well as with the dose (Figure 3B) indicating apoptosis as mode of 2_{mG} induced cell death. Starved and/or heat shocked cells were always used as compensation controls for Annexin V-FITC and PI staining for all performed experiments.

One of the most common signaling cascades involved in apoptosis is the activation of a highly specialized family of cysteinyl-aspartate proteases (caspases), which are usually present in the inactive zymogen forms. Once activated, caspases initiate cell death by cleaving and thus activating effector caspases, which drive the process of apoptosis (Li and Yuan 2008). Caspase mediated apoptotic cell death is accomplished through the cleavage of several key proteins required for cellular functioning and survival (Fischer et al 2003). PARP-1 is one of the several known cellular substrates of caspases. Cleavage of PARP-1 by caspases is considered to be the hallmark of apoptosis (Kaufmann et al 1993, Tewari et al 1995). In order to test our conclusion that 2_{mG} induces apoptosis, formulated based on the data from Figure 3A and 3B, we treated HeLa cells with 22 μM concentration of the complex

during 24-72 h. Our data showed that 2_{mG} does not induce PARP cleavage, which was detected in HeLa cells treated 72 h with 5 μ M cisplatin (cDDP) used as a positive control (Figure 3C). Moreover, the pre-treatment of HeLa cells with pan caspase inhibitor that irreversibly binds to the catalytic site of caspase proteases and can inhibit the induction of apoptosis, carbobenzoxy-valyl-alanyl-aspartyl-[O-methyl]-fluoromethylketone (Z-VAD), did not protect cells from 2_{mG} induced cell death (Figure 3D). Additionally, the caspase independent cell death was confirmed upon specifically measuring caspase 3 and 7 activity in the HeLa cells treated 48 and 72 h with 22 μ M 2_{mG} (Figure S12A), and by two hours pre-treatment of additional cell system, HEp2 cells, with Z-VAD prior to treatment with 2_{mG} (Figure S12B). The activity of caspase 3/7 upon 2_{mG} treatment was not detected (Figure S12A) and Z-VAD did not increase survival of HEp2 cell line upon 2_{mG} treatment (Figure S12B). The fact that we did not detect cleavage of PARP and that Z-VAD did not prevent 2_{mG} induced cell death brought us to the hypothesis that 2_{mG} probably induces caspase independent cell death. The pre-treatment of cells with inhibitor of necroptosis, necrostatin-1 (Vandenabeele et al 2013), did not protect cells from death (Figure S13), excluding this type of cell death from the involvement in the 2_{mG} toxicity.

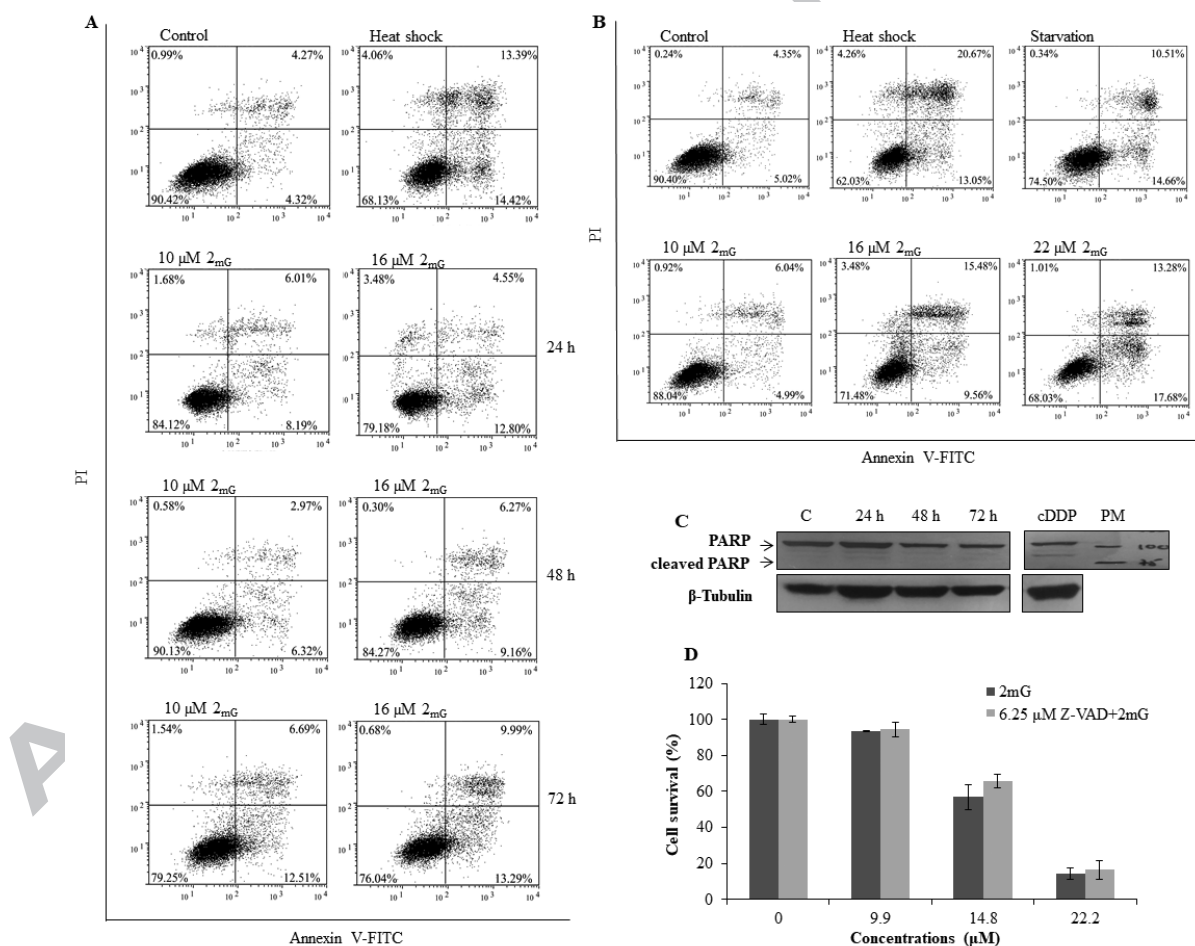


Figure 3. 2_{mG} compound induces cell death in HeLa cells. Cells were treated either with 10 or 16 μ M 2_{mG} for 24-72 h (A) or 10, 16 and 22 μ M 2_{mG} for 72 h (B). The cell death was measured by flow cytometry. The one of three performed experiments for each set of conditions is shown. Starved (24 h cell growth without serum) or heat shocked (10 min, 56 $^{\circ}$ C) cells were always used as a compensation Annexin V-FITC/PI controls. PI-/Annexin V-

FITC- cells (lower left quadrant), PI-/Annexin V-FITC+ cells (lower right quadrant), PI+/Annexin V-FITC+ cells (upper right quadrant). Cleavage of PARP was detected by Western blot. β -Tubulin was used as a loading control. One out of three performed experiments is presented. HeLa cells treated with 5 μ M cisplatin (cDDP) during 72 h were used as positive control for PARP cleavage (C). HeLa cells were pre-treated for two hours with 6.25 μ M Z-VAD prior to treatment with different concentrations of 2_{mG} . The cell survival was measured 72 h after the treatment by MTT assay. The experiments were repeated at least three times (D).

From the literature is known that cells can enter autophagy prior to dying (Dikic and Elazar 2018, Levine and Kroemer 2008). Autophagy is a homeostatic cellular process regulating protein and organelle turnover by lysosomal destruction (Levine and Kroemer 2008). The treatment of HeLa cells with 22 μ M 2_{mG} during 24-72 h induced increase in Beclin-1, which is accompanied with the increase of proteolytic derivate LC3-II visible upon 72 h treatment (**Figure 4A**). This is in line with the fact that Beclin-1 is involved in autophagosome formation and LC3 is located in the cytosol (LC3-I) or in autophagosomal membranes (LC3-II). LC3-II may thus be used to estimate the abundance of autophagosomes prior to their destruction through fusion with lysosomes (Klionsky et al 2012). With the intention to verify the possible role of autophagy in 2_{mG} induced cell death, the cells were pretreated with bafilomycin A (BAF A), which is a known inhibitor of the late phase of autophagy (Klionsky et al 2012), and then treated with different concentrations of 2_{mG} . BAF A decreased the toxic effect of 2_{mG} (**Figure 4B**) pointing towards the conclusion that 2_{mG} induces autophagy. Additional inhibitor of autophagy, 3-methyladenine (3-MA), which is an inhibitor of phosphatidylinositol 3-kinases (PI3K), decreased the toxicity of 2_{mG} as well (**Figure S11**). PI3K plays an important role in many biological processes, including controlling the activation of the mechanistic target of rapamycin (mTOR), a key regulator of autophagy (Wu et al 2010). Autophagy as the mode of cell death upon 2_{mG} treatment was confirmed in HEP2 cell line by MTT and SRB assays (**Figure S14A** and **S14B**). The obtained data imply the autophagy as a part of 2_{mG} triggered caspase independent programmed cell death. There are multiple caspase-dependent and -independent mechanisms by which classical features of programmed cell death are mediated (Liu et al 2003). Further investigation is needed to understand 2_{mG} triggered caspase independent programmed cell death and the correlation of autophagy with it.

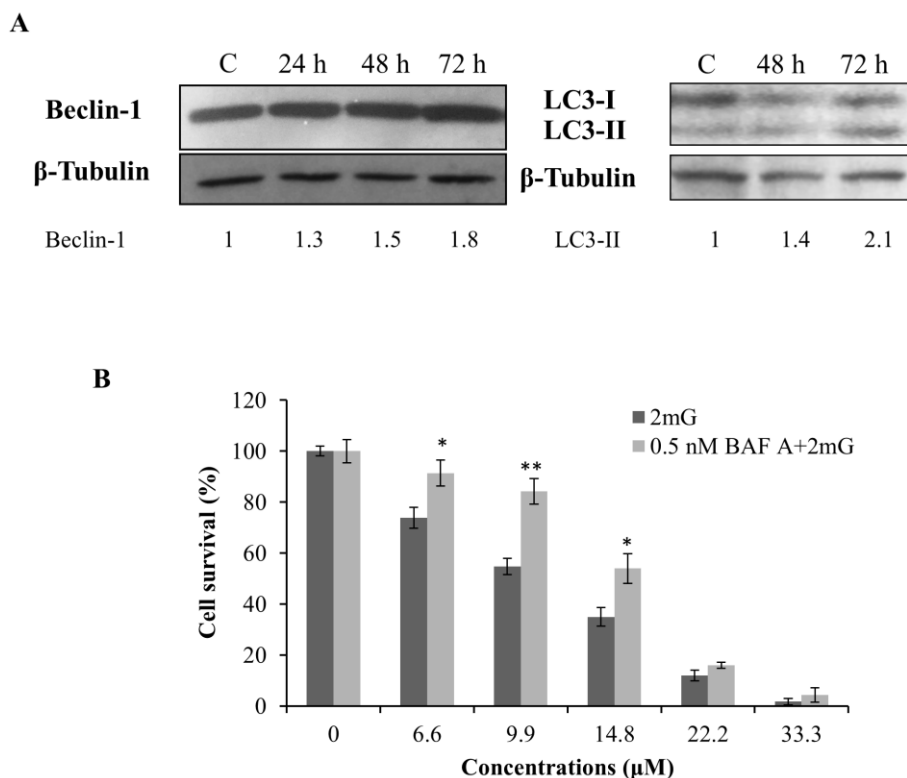


Figure 4. 2_{mG} compound induces autophagy in HeLa cells. Cells were treated with $22 \mu M$ 2_{mG} . The expression of Beclin-1, LC3-I and LC3-II was detected by Western blot. β -Tubulin was used as a loading control. Data obtained with densitometric analysis are expressed as a ratio between examined Beclin-1 or LC3-II and β -Tubulin. Non-treated cells were set as 1.0. One out of three performed experiments for each protein is presented (A). HeLa cells were pre-treated for two hours either with $6.25 \mu M$ Z-VAD or with $0.5 nM$ BAF A prior to treatment with different concentrations of 2_{mG} . The cell survival was measured 72 h after the treatment by MTT assay. The experiments were repeated at least three times. Significance was determined between the 2_{mG} only and either Z-VAD or BAF A pre-treated and 2_{mG} treated cells (*, $P < 0.05$; **, $P < 0.01$) (B).

The role of glutathione. The fact that cancer cells are generally growing and multiplying much faster than normal healthy cells and have a rapid production of new biomolecules, makes them more vulnerable to compounds such as the one investigated. Also, tumor cells produce a reductive environment due to the increased metabolic rate, feature that opens the possibility to activate ruthenium complexes solely at the site of cancerous cells (Antonarakis and Emadi 2010). The tripeptide GSH has the capacity to bind different metal-based drugs (Brozovic et al 2010). We were interested in the possibility that GSH is involved in detoxification of investigated compounds due to their capacity to bind proteins (Table 3). For that purpose, HeLa cells were either pre-treated with specific inhibitor of GSH synthesis, $0.01 \mu g/mL$ buthionine sulfoximine (BSO) overnight or with precursor of GSH synthesis, $5 mM$ N-acetylcysteine (NAC) for two hours prior to treatment with 2_{pG} , 2_{pA} , 2_{mG} or 2_{mA} . The conditions used were tested previously to be effective (Brozovic et al 2008, Brozovic et al 2014). The obtained data showed decreased survival of HeLa cells in the case when GSH was depleted by BSO and increased survival of cells in the case when the level of GSH was increased due to the NAC (Figure 5A-D). Similar results were obtained for all examined bis-

ruthenium complexes, showing the importance of GSH in the toxicity of examined compounds.

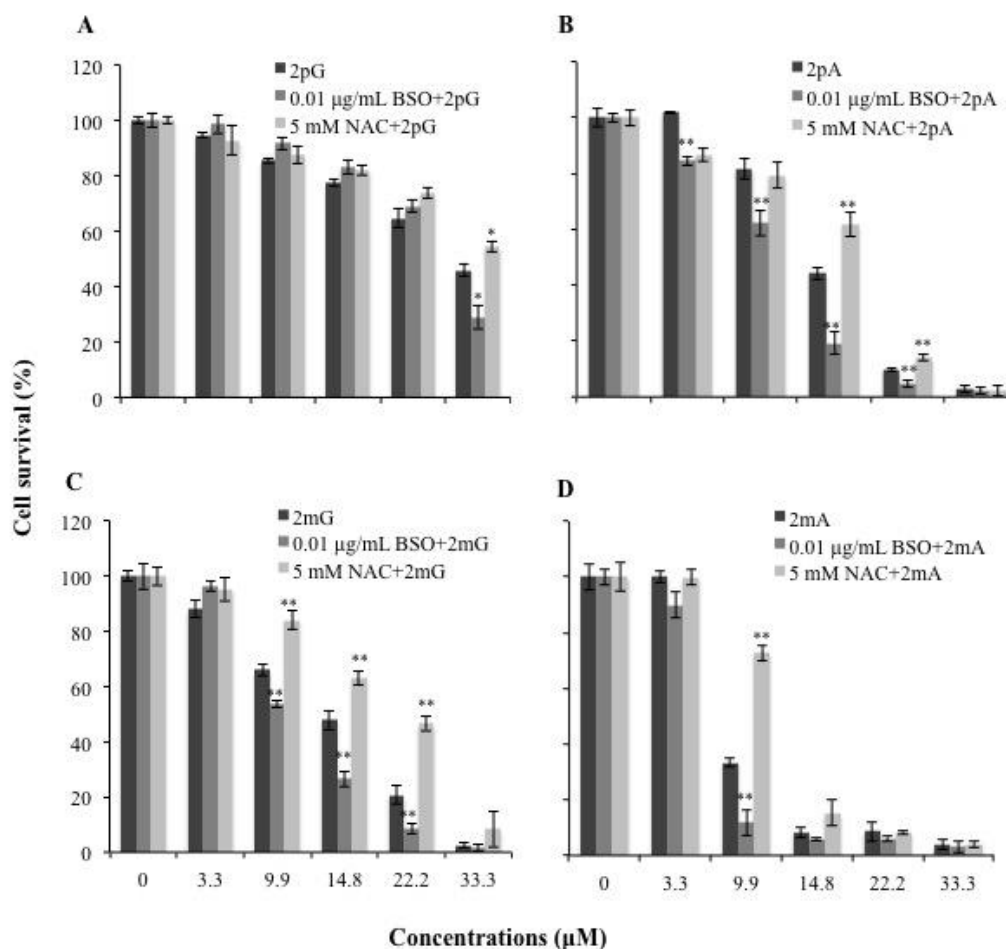


Figure 5. Glutathione reduced the toxicity of 2_{pG}, 2_{pA}, 2_{mG} and 2_{mA}. HeLa cells were pre-treated either with 0.01 μg/mL BSO (overnight) or with 5 mM NAC (2 h) prior to treatment with different concentrations of 2_{pG} (A), 2_{pA} (B), 2_{mG} (C) or 2_{mA} (D). The cell survival was measured 72 h after the treatment by MTT assay. The experiments were repeated at least three times. Significance was determined between the 2_{mG} only and either BSO or NAC pre-treated and 2_{pG}/2_{pA}/2_{mG}/2_{mA} treated cells (*, P < 0.05; **, P < 0.01).

Since GSH is one of the major endogenous antioxidants, we next measured the formation of reactive oxygen species (ROS) upon treatment of HeLa cells with 2_{mG}. We were not able to detect increased formation of ROS (Figure S12A and S12B) by flow cytometry, what is in line with our prediction that this type of chemical structure does not activate the formation of ROS. Therefore, we concluded that GSH probably has a role, not as an antioxidant, but rather as a detoxification mechanism in the cells. This hypothesis was confirmed with pre-treatment of cells with two antioxidant compounds, tempol and trolox, which did not protect cells from 2_{mG} toxicity (Figures S13A and S13B). The combination treatment of HeLa cells with well accepted inhibitor of glutathione S-transferase (GST) (a detoxification enzymes that catalyze the conjugation of GSH to a wide variety of endogenous and exogenous electrophilic compounds) (Townsend and Tew 2003), 5 or 7.5 μg/mL ethacrynic acid (ETA) (Osmak et al 1998), decreased cell survival compared with cells treated with 2_{mG} only (Figure 6A). The

data implied enzymatically-regulated formation of detoxification complex between GSH and 2_{mG} . Moreover, pre-treatment of HeLa cells with probenecid, the inhibitor of MRP/GS-X pumps (Zaman et al 1995), decreased survival of cells compared to the ones treated only with 2_{mG} (**Figure 6B**). These results indicate efflux of the formed conjugates out of the cells and the detoxification role of GSH.

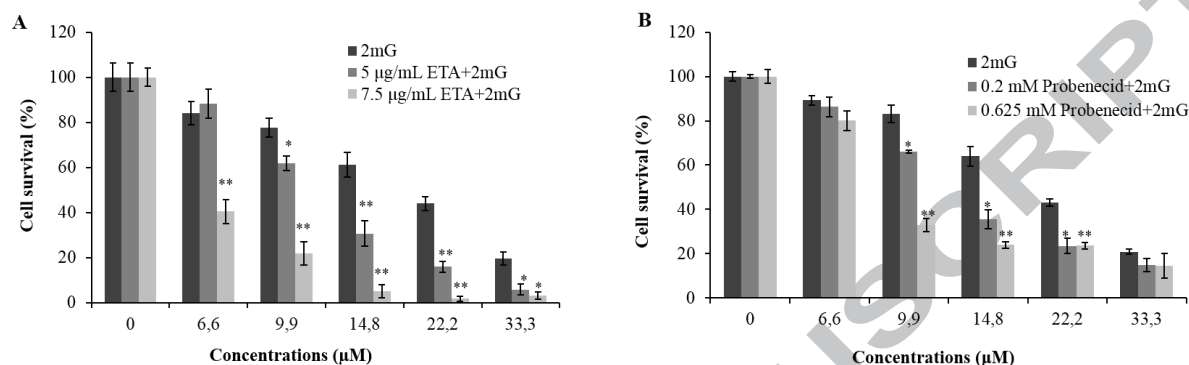


Figure 6. Glutathione probably forms conjugates with the 2_{mG} . HeLa cells were pre-treated either with 5 or 7.5 µg/mL ETA (A) or with 0.2 or 0.625 mM probenecid (B) prior to treatment with different concentrations of 2_{mG} . The cell survival was measured 72 h after by MTT assay. The experiments were repeated at least three times. Significance was determined between the 2_{mG} only and either ETA or probenecid pre-treated and 2_{mG} treated cells (*, $P < 0.05$; **, $P < 0.01$).

Cellular accumulation. Further we were interested to check the correlation between cellular accumulations of investigated compounds with their toxicity (Pongratz et al 2004, Puckett et al 2010). The HeLa cells were treated with 150 µM 2_{pG} , 2_{pA} , 2_{mG} or 2_{mA} during 2-6 h and analyzed by high-resolution inductively coupled plasma mass spectrometry (HR ICPMS). Our results showed that the amount of ruthenium in the cells is the highest upon treatment with 2_{pA} and the lowest upon treatment with 2_{mG} (**Figure 7A**). The obtained data were further confirmed by investigation of dose-dependent accumulation of ruthenium for all compounds (**Figure 7B**). The data also showed that the amount of ruthenium does not correlate with toxicity of each compound (**Table 1**). In a line with that, compound 2_{mG} , used for most of the testing, was well chosen since it exhibits significant toxicity (**Table 1**) with the lowest amount of ruthenium in the cell. The most likely reasons, which need further investigation, could be different structural features of the compounds, which regulate different cellular uptake or even different capacity of GSH to detoxify them. The fact that hydrophobicity is an important pharmacological feature, closely related to the drug uptake and efflux, and the fact that phenyl group is hydrophobic (Liu et al 2011) could explain why phenyl group in *para*-position (2_{pA}) correlates with accumulation and in *meta*-position (2_{mA}) with toxicity. By using the same model system, HeLa cells, it was shown that anti-metastatic effect of NAMI-A is unrelated to the penetration of the compound in the cell (Sava et al 2004). The extent of ruthenium uptake of three complexes did not correlate with their different cytotoxicity in ovarian cancer A2780 cell line (Bugarcic et al 2008, Komor and Barton 2013).

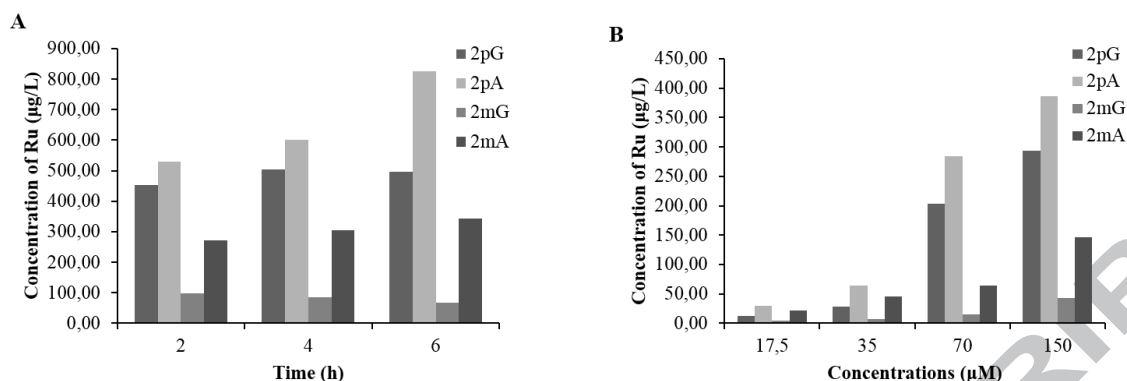


Figure 7. The accumulation of 2_{pG} , 2_{pA} , 2_{mG} and 2_{mA} in HeLa cells is different. The HeLa cells were either treated with 150 μM concentration of 2_{pG} , 2_{pA} , 2_{mG} or 2_{mA} from two to six hours (A) or with 17.5-150 μM during two hours (B). The cells were collected at the indicated time points and the amount of ruthenium was measured by HR ICPMS. Two out of four independent experiments are presented.

Conclusions.

In this study, six triphenylphosphine ligands (**L**) conjugated to amino acids and ten ruthenium(II)-cymene complexes thereof, including both **ML** and **ML₂** stoichiometry, were prepared, purified and characterized by NMR (¹H, ¹³C, ³¹P), CD and MS techniques and DFT calculations (wB97xD, gas phase). Cytotoxicity screening using human cervical carcinoma (HeLa) cells and MTT assay revealed the IC₅₀ value of 5-30 μM for all examined **ML₂** complexes (2_{pG} , 2_{pA} , 2_{mG} and 2_{mA}), while for all other compounds (**L**, **ML** and Ru precursor) the IC₅₀ values were above 33.3 μM . Additional analysis performed with 2_{mG} showed similar toxicity on several other human carcinomas (laryngeal carcinoma HEP2, lung carcinoma H460, and breast carcinoma MDA-MB-231), but no toxicity for normal human cell lines (both keratinocytes and fibroblasts). Studies of non-covalent interactions (thermal melting, CD and fluorescence titrations) of ruthenium complexes with *ct*-DNA and BSA, as model systems for potential biomolecular targets, revealed no measurable interaction with DNA, but a micromolar affinity for proteins. Interestingly, bioconjugates with lower IC₅₀ values showed higher binding affinities towards BSA.

Further evaluation of biological activity showed that 2_{mG} increased cells in S phase and subsequently decreased them in G1 phase of the cell cycle, what was followed by increase of the SubG0/G1 cell fraction. Staining with Annexin V-FITC and PI indicated programmed cell death as a mode of 2_{mG} action. Caspase independent cell death was deduced from (a) the lack of PARP-1 cleavage and (b) existence of cell death despite the Z-VAD presence. In addition, a similar effect obtained by pre-treatment of cells with necrostatin-1 indicated absence of necroptosis, as another possible mode of cell death. Increase of Beclin-1 as well as LC3-II expression indicated that 2_{mG} induced autophagy as part of cell death. Moreover, the autophagy inhibitors BAF-A and 3-MA decreased the toxic effect of 2_{mG} , confirming the involvement of autophagy in its toxic effect.

Importance of GSH in the cell response to all **ML₂** complexes (2_{pG} , 2_{pA} , 2_{mG} and 2_{mA}) was shown using BSO and NAC, revealing decreased (BSO) and increased (NAC) survival, respectively. Detoxification role of GSH was suggested by the absence of ROS formation and

no effect of two antioxidants, tempol and trolox, on cell survival. On the other hand, increased survival was detected when ethacrynic acid was used, indicating detoxification role of GSH. This was further confirmed with inhibition of GSH-**2_{mG}** conjugates efflux by probenecid, which had the same effect on cell survival. Cellular uptake, analyzed by HR ICPMS, showed different dose- and time-dependent cellular accumulation of the studied complexes. It is particularly interesting to mention that *para*-substituted complexes (**2_{pG}** and **2_{pA}**) are characterized by higher uptake into the cell, while *meta*-substituted complexes (**2_{mG}** and **2_{mA}**) are more toxic.

Here, we described for the first time newly synthesized ruthenium complexes which are causing non oxidative protein damage and trigger autophagy, and also induce cells protection mechanism through GSH led detoxification. Taken together, **ML₂** complexes deserve further investigation as potential chemotherapeutic agents for different types of cancer.

Experimental.

General. Reactions were carried out in ordinary glassware and chemicals were used as purchased from commercial suppliers without further purification. Reactions were monitored by TLC on Silica Gel 60 F254 plates and detected with UV lamp (254 nm); organic compounds were purified using automated flash chromatography equipped with a UV detector (254 nm) and prepacked silica columns. NMR spectra were obtained on spectrometer operating at 300.13 or 600.13 MHz for ¹H, 242.92 MHz for ³¹P and 150.92 MHz for ¹³C nuclei. Mass spectra were measured on a HPLC-MS system coupled with 6410 triple-quadrupole mass spectrometer, operating in a positive ESI mode. High-resolution mass spectra were obtained on a MALDI TOF-TOF instrument using a CHCA matrix. The CD spectra were recorded on a JASCO J-810 spectropolarimeter equipped with Peltier thermostat, using 1 cm Suprasil quartz cells with a scanning speed of 200 nm min⁻¹. The buffer background was subtracted from each spectrum, while each spectrum was a result of three accumulations. The electronic absorption spectra of ruthenium complexes and thermal melting experiments were measured on a Varian Cary 100 Bio spectrometer. Fluorescence titrations were recorded on Varian Cary Eclipse fluorimeter. UV-Vis and fluorescence spectra were recorded using appropriate 1 cm path quartz cuvettes.

Ligands, general procedure. The corresponding 4-(Diphenylphosphino)benzoic acid (1 mmol) was dissolved in dichloromethane (50 mL). HOBt × H₂O (1 mmol), TBTU (1 mmol) and DIPEA (0.5 mL, 4 mmol) were added and the mixture was left stirring at room temperature. After 1 h methyl ester (1 mmol) was added and the mixture was left stirring for the indicated period. After that, the reaction mixture was washed with NaHCO₃ (3 × 50 mL, sat. aq.) and subjected to flash chromatography (hexane/EtOAc).

Ph₂P-*p*C₆H₄-CO-Gly-OMe, L_{pG}; (Kokan and Kirin 2012). 4-(Diphenylphosphino)benzoic acid (301.6 mg, 1 mmol), dichloromethane (50 mL), HOBt × H₂O (135.5 mg, 1 mmol), TBTU (322.1 mg, 1 mmol), DIPEA (0.5 mL, 4 mmol) and H-Gly-OMe × HCl (129.4 mg, 1 mmol), 72 h. Yield: 332.1 mg (88 %). ¹H NMR (300.13 MHz, CDCl₃) δ/ppm: 7.75 (dd, 2H, J₁ = 8.5 Hz, J₂ = 1.5 Hz), 7.26–7.37 (m, 12 H), 6.62 (t, 1H, J = 4.5 Hz), 4.25 (d, 2H, J = 5 Hz), 3.8 (s, 3H).

Ph₂P-*p*C₆H₄-CO-Ala-OMe, L_{pA}; (Kokan et al 2014). 4-(Diphenylphosphino)benzoic acid (302.3 mg, 1 mmol), dichloromethane (50 mL), HOBt × H₂O (134.2 mg, 1 mmol), TBTU

(320.3 mg, 1 mmol), DIPEA (0.5 mL, 4 mmol), H-Ala-OMe \times HCl (132.1 mg, 1 mmol), 24 h. Yield: 296.7 mg (76 %). ^1H NMR (300.13 MHz, CDCl_3) δ /ppm: 7.73–7.76 (m, 2H), 7.26–7.37 (m, 12H), 6.70 (d, 1H, $J = 7$ Hz), 4.75–4.84 (m, 1H), 3.79 (s, 3H), 1.51 (d, 3H, $J = 7$ Hz).

Ph₂P-*m*C₆H₄-CO-Gly-OMe, L_{pG}. 3-(Diphenylphosphino)benzoic acid (305.5 mg, 1 mmol), dichloromethane (50 mL), HOBt \times H₂O (136.7 mg, 1 mmol), TBTU (322.3 mg, 1 mmol), DIPEA (0.5 mL, 4 mmol), H-Gly-OMe \times HCl (127.2 mg, 1 mmol), 24 h. Yield: 291.8 mg (77 %). ^1H NMR (300.13 MHz, CDCl_3) δ /ppm: 7.75–7.82 (m, 2H), 7.26–7.44 (m, 12H), 6.51–6.55 (m, 1H), 4.20 (d, 2H, $J = 5$ Hz), 3.79 (s, 3H). ^{13}C NMR (CDCl_3 , 75.46 MHz) δ /ppm: 41.9 (C α), 52.6 (OMe), 127.7 (C4), 128.8 (d, $^3J_{\text{CP}} = 7$ Hz, C3'), 129.0 (d, $^2J_{\text{CP}} = 5.5$ Hz, C5), 129.2 (C4'), 132.3 (d, $^2J_{\text{CP}} = 24$ Hz, C2), 133.9 (d, $^2J_{\text{CP}} = 20$ Hz, C2'), 134.0 (C3, overlapped with C2' peak), 136.5 (d, $^1J_{\text{CP}} = 11$ Hz, C1'), 136.9 (d, $^2J_{\text{CP}} = 16$ Hz, C6), 138.7 (d, $^1J_{\text{CP}} = 13.5$ Hz, C1), 167.3 (C(O)NH), 170.5 (COOMe). ^{31}P NMR (CDCl_3 , 242.93 MHz) δ /ppm: -4.81 (s, 1P).

Ph₂P-*m*C₆H₄-CO-Ala-OMe, L_{pA}; (Kokan et al 2014). 3-(Diphenylphosphino)benzoic acid (304.1 mg, 1 mmol), dichloromethane (50 mL), HOBt \times H₂O (136.2 mg, 1 mmol), TBTU (321.7 mg, 1 mmol), DIPEA (0.5 mL, 4 mmol), H-Ala-OMe \times HCl (142.3 mg, 1 mmol), 24 h. Yield: 300.1 mg (77 %). ^1H NMR (300.13 MHz, CDCl_3) δ /ppm: 7.76–7.80 (m, 2H), 7.26–7.44 (m, 12H), 6.61 (d, 1H, $J = 8$), 4.70–4.80 (m, 1H), 3.77 (s, 1H), 1.48 (d, 3H, $J = 7$ Hz).

Ph₂P-C₂H₄-CO-Gly-OMe, L_{aG}. 3-(Diphenylphosphino)propionic acid (262.3 mg, 1 mmol), dichloromethane (50 mL), HOBt \times H₂O (136.4 mg, 1 mmol), TBTU (324.3 mg, 1 mmol), DIPEA (0.5 mL, 4 mmol), H-Gly-OMe \times HCl (127.2 mg, 1 mmol), 24 h; Rf (Hexane/EtOAc = 7:3) = 0.10. Yield: 310.2 mg (94 %). ^1H NMR (300.13 MHz, CDCl_3) δ /ppm: 2.26–2.43 (m, 4H), 3.75 (s, 3H), 4.01 (d, $J = 5$ Hz, 2H), 5.93 (t, $J = 4$ Hz, 1H), 7.31–7.36 (m, 6H), 7.39–7.46 (m, 4H). ^{13}C NMR (CDCl_3 , 75.46 MHz) δ /ppm: 23.4 (d, $^1J_{\text{CP}} = 12$ Hz, C1 phosphine), 32.6 (d, $^2J_{\text{CP}} = 18.5$ Hz, C2 phosphine), 41.4 (C α), 52.5 (OMe), 128.7 (d, $^3J_{\text{CP}} = 7$ Hz, C3' phosphine), 129.0 (C4 phosphine), 132.9 (d, $^2J_{\text{CP}} = 18.5$ Hz, C2' phosphine), 137.9 (d, $^1J_{\text{CP}} = 12.5$ Hz, C1' phosphine), 170.6 (COOMe), 172.5 (d, $^3J_{\text{CP}} = 13.5$ Hz, C(O)NH).

Ph₂P-C₂H₄-CO-Ala-OMe, L_{aA}. 3-(Diphenylphosphino)propionic acid (261.9 mg, 1 mmol), dichloromethane (50 mL), HOBt \times H₂O (136.9 mg, 1 mmol), TBTU (327.3 mg, 1 mmol), DIPEA (0.5 mL, 4 mmol), H-Ala-OMe \times HCl (145.3 mg, 1 mmol), 24 h. Rf (Hexane/EtOAc = 7:3) = 0.13. Yield: 273.7 mg (80 %). ^1H NMR (300.13 MHz, CDCl_3) δ /ppm: 1.37 (d, $J = 7$ Hz, 3H), 2.23–2.41 (m, 4H), 3.74 (s, 3H), 4.52–4.61 (m, 1H), 5.97 (d, $J = 7$ Hz, 1H), 7.31–7.36 (m, 6H), 7.39–7.46 (m, 4H). ^{13}C NMR (CDCl_3 , 75.46 MHz) δ /ppm: 18.7 (C β), 23.4 (d, $^1J_{\text{CP}} = 12$ Hz, C1 phosphine), 32.7 (d, $^2J_{\text{CP}} = 18.5$ Hz, C2 phosphine), 48.2 (C α), 52.6 (OMe), 128.7 (d, $^3J_{\text{CP}} = 7$ Hz, C3' phosphine), 128.93, 128.95 (C4 phosphine), 132.86, 132.89 (d, $^2J_{\text{CP}} = 18.5$ Hz, C2' phosphine), 137.89, 137.96 (d, $^1J_{\text{CP}} = 13$ Hz, C1' phosphine), 171.8 (d, $^3J_{\text{CP}} = 14$ Hz, C(O)NH), 173.7 (COOMe). ^{31}P NMR (CDCl_3 , 242.93 MHz) δ /ppm: -14.94 (s, 1P).

ML complexes, general procedure. Ligand **L** was dissolved in DCM (3 mL), di- μ -chlorobis[*p*-cymene]chlororuthenium(II) was added and stirred for 2 h. After the reaction, the crude product was purified by column chromatography on a short silica column (10 g), eluent DCM/MeOH.

[(iPr-*p*C₆H₄-Me)RuCl₂(Ph₂P-*p*C₆H₄-CO-Gly-OMe)], 1_{pG}. Ligand **L_{pG}** (201.5 mg, 0.53 mmol) and di- μ -chlorobis[*p*-cymene]chlororuthenium(II) (142.3, 0.23 mmol); eluent DCM/MeOH 2 %, Rf (DCM/MeOH 3 %) = 0.28. Yield: 279.9 mg (89 %). ^1H NMR (300.13

MHz, CDCl₃) δ /ppm: 7.69–7.95 (m, 8H), 7.37–7.47 (m, 6H), 6.64 (t, 1H, $J = 5$ Hz), 5.22 (d, 2H, $J = 6$ Hz), 4.98 (d, 2H, $J = 6$ Hz), 4.21 (d, 2H, $J = 5$ Hz), 3.78 (s, 3H), 3.49 (d, 1H, $J = 5.5$ Hz), 2.81–2.91 (m, 1H), 1.86 (s, 3H), 1.12 (d, 6H, $J = 7$ Hz). ¹³C NMR (CDCl₃, 150.92 MHz) δ /ppm: 18.0 (CH₃, cymene), 22.0 (CHCH₃, cymene), 30.4 (CHCH₃, cymene), 41.9 (C α), 52.6 (OMe), 87.5 (d, ² $J_{CP} = 5.5$ Hz, C2, C6, cymene), 89.0 (d, ² $J_{CP} = 3$ Hz, C3, C5, cymene), 96.4 (C4, cymene), 111.6 (d, ² $J_{CP} = 3.5$ Hz, C1, cymene), 126.5 (d, ³ $J_{CP} = 10$ Hz, C3, phosphine), 128.4 (d, ³ $J_{CP} = 10$ Hz, C3', phosphine), 130.7 (C4', phosphine), 133.5 (d, ¹ $J_{CP} = 45$ Hz, C1', phosphine), 134.3 (d, ² $J_{CP} = 9.5$ Hz, C2', phosphine), 134.8 (d, ² $J_{CP} = 9.5$ Hz, C2, phosphine), 135.1 (C4, phosphine), 137.7 (d, ¹ $J_{CP} = 44$ Hz, C1, phosphine), 167.1 (C(O)NH), 170.4 (COOMe). ³¹P NMR (CDCl₃, 242.93 MHz) δ /ppm: 25.32 (s, 1P). MALDI-HRMS (m/z): calcd 613.1320 (C₃₂H₃₄NO₃PRu⁺), found 613.1329.

[(iPr-*p*C₆H₄-Me)RuCl₂(Ph₂P-*p*C₆H₄-CO-Ala-OMe)], **1_{pA}**. Ligand **L_{pA}** (191 mg, 0.49 mmol) and di- μ -chlorobis[(*p*-cymene)chlororuthenium(II)] (131.2, 0.21 mmol); eluent DCM/MeOH 2 %, Rf (DCM/MeOH 3 %) = 0.28. Yield: 218.3 mg (75 %). ¹H NMR (300.13 MHz, CDCl₃) δ /ppm: 7.69–7.95 (m, 8H), 7.37–7.47 (m, 6H), 6.67 (d, 1H, $J = 7.5$ Hz), 5.21–5.24 (m, 2H), 4.98 (d, 2H, $J = 6$ Hz), 4.71–4.80 (m, 1H), 3.77 (s, 3H), 2.8–2.93 (m, 1H), 1.87 (s, 3H), 1.49 (d, 3H, $J = 7$ Hz), 1.12 (d, 6H, $J = 7$ Hz). ¹³C NMR (CDCl₃, 150.92 MHz) δ /ppm: 18.0 (CH₃, cymene), 18.6 (C β), 22.0 (CHCH₃, cymene), 30.4 (CHCH₃, cymene), 48.7 (C α), 52.7 (OMe), 87.48, 87.52 (d, ² $J_{CP} = 5$ Hz, C2, C6, cymene), 88.99, 89.04 (d, ² $J_{CP} = 3$ Hz, C3, C5, cymene), 96.3 (C4, cymene), 111.6 (d, ² $J_{CP} = 3.5$ Hz, C1, cymene), 126.4 (d, ³ $J_{CP} = 10$ Hz, C3, phosphine), 128.3 (d, ³ $J_{CP} = 10$ Hz, C3', phosphine), 130.7 (C4', phosphine), 133.51, 133.52 (d, ¹ $J_{CP} = 45$ Hz, C1', phosphine), 134.4 (d, ² $J_{CP} = 9.5$ Hz, C2', phosphine), 134.8 (d, ² $J_{CP} = 9.5$ Hz, C2, phosphine), 135.28, 135.29 (C4, phosphine), 137.7 (d, ¹ $J_{CP} = 44.5$ Hz, C1, phosphine), 166.5 (C(O)NH), 173.4 (COOMe). ³¹P NMR (CDCl₃, 242.93 MHz) δ /ppm: 25.31 (s, 1P). MALDI-HRMS (m/z): calcd 662.1165 (C₃₃H₃₆ClNO₃PRu⁺), found 662.1131.

[(iPr-*p*C₆H₄-Me)RuCl₂(Ph₂P-*m*C₆H₄-CO-Gly-OMe)], **1_{mG}**. Ligand **L_{mG}** (182.2 mg, 0.48 mmol) and di- μ -chlorobis[(*p*-cymene)chlororuthenium(II)] (147.1, 0.24 mmol); eluent DCM/MeOH 2 %, Rf (DCM/MeOH 3 %) = 0.26. Yield: 301.1 mg (92 %). ¹H NMR (300.13 MHz, CDCl₃) δ /ppm: 8.83 (dt, 1H, $J_1 = 12$ Hz, $J_2 = 1.5$ Hz), 7.78–7.91 (m, 5H), 7.56–7.63 (m, 1H), 7.31–7.49 (m, 7H), 6.93 (t, 1H, $J = 5.5$ Hz), 5.22 (d, 2H, $J = 6$ Hz), 5.07 (d, 2H, $J = 6$ Hz), 5.19 (d, 2H, $J = 5.5$ Hz), 3.77 (s, 3H), 2.77–2.86 (m, 1H), 1.88 (s, 3H), 1.08 (d, 6H, $J = 7$ Hz). ¹³C NMR (CDCl₃, 150.92 MHz) δ /ppm: 17.9 (CH₃, cymene), 21.9 (CHCH₃, cymene), 30.4 (CHCH₃, cymene), 41.9 (C α), 52.4 (OMe), 87.2 (d, ² $J_{CP} = 5.5$ Hz, C2, C6, cymene), 89.5 (d, ² $J_{CP} = 2.5$ Hz, C3, C5, cymene), 96.2 (C4, cymene), 111.6 (d, ² $J_{CP} = 2.5$ Hz, C1, cymene), 128.3 (d, ³ $J_{CP} = 8.5$ Hz, C5, phosphine), 128.5 (d, ³ $J_{CP} = 9.5$ Hz, C3', phosphine), 129.8 (C4, phosphine), 130.8 (C4', phosphine), 132.4 (d, ¹ $J_{CP} = 46$ Hz, C1', phosphine), 132.9 (d, ³ $J_{CP} = 11$ Hz, C3, phosphine), 133.9 (d, ² $J_{CP} = 9.5$ Hz, C2', phosphine), 134.1 (d, ¹ $J_{CP} = 46$ Hz, C1, phosphine), 135.2 (d, ² $J_{CP} = 16$ Hz, C2, phosphine), 136.73, 136.75 (C6, phosphine), 167.2 (C(O)NH), 170.3 (COOMe). ³¹P NMR (CDCl₃, 242.93 MHz) δ /ppm: 25.50 (s, 1P). +ESI MS (m/z): 648.1 ([M – Cl]⁺, 81 %). MALDI-HRMS (m/z): calcd 612.1241 (C₃₂H₃₃NO₃PRu⁺), found 612.1226.

[(iPr-*p*C₆H₄-Me)RuCl₂(Ph₂P-*m*C₆H₄-CO-Ala-OMe)], **1_{mA}**. Ligand **L_{mA}** (180 mg, 0.46 mmol) and di- μ -chlorobis[(*p*-cymene)chlororuthenium(II)] (141.6, 0.23 mmol); eluent DCM/MeOH 2 %, Rf (DCM/MeOH 3 %) = 0.28. Yield: 302 mg (94 %). ¹H NMR (300.13 MHz, CDCl₃) δ /ppm: 8.75–8.80 (m, 1H), 7.76–7.78 (m, 5H), 7.61–7.68 (m, 1H), 7.31–7.47 (m, 7H), 6.88 (d, 1H, $J = 8$ Hz), 5.26–5.30 (m, 2H), 5.17 (d, 2H, $J = 6.5$ Hz), 4.96 (d, 2H, $J = 6$

Hz), 4.65–4.75 (m, 1H), 3.76 (s, 3H), 2.75–2.89 (m, 1H), 1.88 (s, 3H), 1.52 (d, 3H, $J = 7$ Hz), 1.08 (t, 6H, $J = 7.5$ Hz). ^{13}C NMR (CDCl_3 , 150.92 MHz) δ/ppm : 17.9 (CH_3 , cymene), 18.3 ($\text{C}\beta$), 21.8, 22.0 (CHCH_3 , cymene), 30.4 (CHCH_3 , cymene), 48.8 ($\text{C}\alpha$), 52.6 (OMe), 86.987.6 (d, $^2J_{\text{CP}} = 5.5$ Hz, C2, C6, cymene), 89.3, 89.4 (d, $^2J_{\text{CP}} = 2.5$ Hz, C3, C5, cymene), 96.3 (C4, cymene), 111.5 (d, $^2J_{\text{CP}} = 3$ Hz, C1, cymene), 128.3 (d, $^3J_{\text{CP}} = 8.5$ Hz, C5, phosphine), 128.5 (d, $^3J_{\text{CP}} = 9.5$ Hz, C3', phosphine), 129.6 (C4, phosphine), 130.8 (C4', phosphine), 132.6 (d, $^1J_{\text{CP}} = 46$ Hz, C1', phosphine), 133.1 (d, $^3J_{\text{CP}} = 11$ Hz, C3, phosphine), 133.9–134.4 (C2', C1, phosphine), 135.1 (d, $^2J_{\text{CP}} = 16$ Hz, C2, phosphine), 136.72, 136.74 (C6, phosphine), 166.5 (C(O)NH), 173.4 (COOMe). ^{31}P NMR (CDCl_3 , 242.93 MHz) δ/ppm : 25.49 (s, 1P). +ESI MS (m/z): 662.1 ($[\text{M} - \text{Cl}]^+$, 100 %). MALDI-HRMS (m/z): calcd 627.1476 ($\text{C}_{33}\text{H}_{36}\text{NO}_3\text{PRu}^+$), found 627.1504.

[(iPr-*p*C₆H₄-Me)RuCl₂(Ph₂P-C₂H₄-CO-Gly-OMe)], 1_{aG}. Ligand L_{aG} (180 mg, 0.55 mmol) and di- μ -chlorobis[*p*-cymene]chlororuthenium(II) (167.9, 0.28 mmol); eluent DCM/MeOH 1 % using 40 g silica, Rf (DCM/MeOH 3 %) = 0.34. Yield: 297.2 mg (85 %). ^1H NMR (300.13 MHz, CDCl_3) δ/ppm : 0.98 (d, $J = 7$ Hz, 6H), 2.21–2.26 (m, 2H), 2.62 (septuplet, $J = 7$ Hz, 1H), 2.88–2.93 (m, 2H), 3.68 (s, 3H), 3.78 (d, $J = 5.5$ Hz, 2H), 5.09 (d, $J = 6$ Hz, 2H), 5.18 (d, $J = 6$ Hz, 2H), 6.21 (t, $J = 5$ Hz, 2H), 7.45–7.50 (m, 6H), 7.78–7.80 (m, 4H). ^{13}C NMR (CDCl_3 , 75.46 MHz) δ/ppm : 17.7 (CH_3 , cymene), 21.8 (CHCH_3 , cymene), 22.9 (d, $^1J_{\text{CP}} = 30$ Hz, C1 phosphine), 30.2 (CHCH_3 , cymene), 30.9 (d, $^2J_{\text{CP}} = 2$ Hz, C2 phosphine), 41.3 ($\text{C}\alpha$), 52.3 (OMe), 86.1 (d, $^2J_{\text{CP}} = 6$ Hz, C2, C6, cymene), 90.1 (d, $^2J_{\text{CP}} = 4$ Hz, C3, C5, cymene), 95.1 (C4, cymene), 109.5 (d, $^2J_{\text{CP}} = 1$ Hz, C1, cymene), 128.6 (d, $^3J_{\text{CP}} = 9$ Hz, C3' phosphine), 130.90, 130.93 (C4' phosphine), 133.3 (d, $^2J_{\text{CP}} = 9$ Hz, C2' phosphine), 133.5 (d, $^1J_{\text{CP}} = 43$ Hz, C1' phosphine), 170.2 (COOMe), 172.6 (d, $^3J_{\text{CP}} = 13$ Hz, C(O)NH). ^{31}P NMR (CDCl_3 , 242.93 MHz) δ/ppm : 21.36 (s, 1P). MALDI-HRMS (m/z): calcd 600.1008 ($\text{C}_{28}\text{H}_{34}\text{ClNO}_3\text{PRu}^+$), found 600.1011.

[(iPr-*p*C₆H₄-Me)RuCl₂(Ph₂P-C₂H₄-CO-Ala-OMe)], 1_{aA}. Ligand L_{aA} (164 mg, 0.48 mmol) and di- μ -chlorobis[*p*-cymene]chlororuthenium(II) (146.3, 0.24 mmol); eluent DCM/MeOH 1 % using 40 g. Yield: 196.8 mg (63 %). ^1H NMR (300.13 MHz, CDCl_3) δ/ppm : 0.96 (d, $J = 7$ Hz, 3H), 0.98 (d, $J = 7$ Hz, 3H), 1.28 (d, $J = 7$ Hz, 3H), 2.06–2.29 (m, 2H), 2.63 (septuplet, $J = 7$ Hz, 1H), 2.85–2.94 (m, 2H), 3.67 (s, 3H), 4.26–4.36 (m, 1H), 5.07–5.11 (m, 2H), 5.17–5.20 (m, 2H), 6.14 (d, $J = 7$ Hz, 1H), 7.43–7.50 (m, 6H), 7.76–7.82 (m, 4H). ^{13}C NMR (CDCl_3 , 75.46 MHz) δ/ppm : 17.7 (CH_3 , cymene), 18.2 ($\text{C}\beta$), 21.7, 21.9 (CHCH_3 , cymene), 22.9 (d, $^1J_{\text{CP}} = 31$ Hz, C1 phosphine), 30.2 (CHCH_3 , cymene), 31.0 (C2 phosphine), 48.2 ($\text{C}\alpha$), 52.4 (OMe), 86.1 (d, $^2J_{\text{CP}} = 5.5$ Hz, C2, C6, cymene), 90.1 (d, $^2J_{\text{CP}} = 4$ Hz, C3, C5, cymene), 95.2 (C4, cymene), 109.5 (d, $^2J_{\text{CP}} = 1$ Hz, C1, cymene), 128.59, 128.62 (d, $^3J_{\text{CP}} = 9.5$ Hz, C3' phosphine), 130.88–130.92 (m, C4' phosphine), 133.3, 133.4 (d, $^2J_{\text{CP}} = 8$ Hz, C2' phosphine), 133.56, 133.62 (d, $^1J_{\text{CP}} = 43$ Hz, C1' phosphine), 172.0 (d, $^3J_{\text{CP}} = 14$ Hz, C(O)NH), 173.3 (COOMe). ^{31}P NMR (CDCl_3 , 242.93 MHz) δ/ppm : 21.35 (s, 1P). MALDI-HRMS (m/z): calcd 614.1165 ($\text{C}_{29}\text{H}_{36}\text{ClNO}_3\text{PRu}^+$), found 614.1180.

ML₂ complexes, general procedure. Mono complex **1** and NH_4PF_6 were dissolved in CH_3CN (5 mL) and refluxed for 35–45 min. CH_3CN was evaporated, the residue dissolved in DCM (5 mL) and filtrated through Celite. Ligand **L** was dissolved in DCM (2 mL), added to the filtrate and the mixture was stirred for 24 h. The crude product was purified by column chromatography on silica (40g), using DCM/MeOH 1 % as eluent.

[(iPr-*p*C₆H₄-Me)RuCl(Ph₂P-*p*C₆H₄-CO-Gly-OMe)₂]PF₆, 2_{pG}. Mono complex **1_{pG}** (51.2 mg, 0.075 mmol), NH_4PF_6 (18.2 mg, 0.11 mmol) and ligand **L_{pG}** (70 mg, 0.19 mmol). Rf

(DCM/MeOH 3 %) 0.18. Yield: 32.6 mg (37 %). ^1H NMR (300.13 MHz, CDCl_3) δ /ppm: 7.23–7.60 (m, 28H), 7.12 (t, 2H, $J = 5.5$ Hz), 5.53 (d, 2H, $J = 4$ Hz), 5.14 (d, 2H, $J = 6$ Hz), 4.21 (d, 4H, $J = 5.5$ Hz), 3.78 (s, 6H), 2.68–2.77 (m, 1H), 1.24 (d, 6H, $J = 7$ Hz), 1.09 (s, 3H). ^{13}C NMR (CDCl_3 , 150.92 MHz) δ /ppm: 15.5 (CH_3 , cymene), 21.6 (CHCH_3 , cymene), 31.6 (CHCH_3 , cymene), 41.9 ($\text{C}\alpha$), 52.5 (OMe), 89.3 (t, $^2J_{\text{CP}} = 5$ Hz, C2, C6, cymene), 97.6 (C3, C5, cymene), 101.0 (C4, cymene), 126.97, 127.01 (d, $^3J_{\text{CP}} = 5$ Hz, C3, phosphine), 128.64, 128.68, 128.85, 128.88 (d, $^3J_{\text{CP}} = 5$ Hz, C3', phosphine), 131.2, 131.6 (C4', phosphine), 131.8 (C1, cymene), 133.2–133.9 (m, C1' phosphine), 134.12, 134.16, 134.26, 134.30, 134.49, 134.52 (d, $^2J_{\text{CP}} = 4$ Hz, C2, C2', phosphine), 136.2 (C4, phosphine), 136.4 (d, $^2J_{\text{CP}} = 45$ Hz, C1, phosphine), 167.2 (C(O)NH), 170.3 (COOMe). ^{31}P NMR (CDCl_3 , 242.93 MHz) δ /ppm: –143.93 (septuplet, hexafluorophosphate), 21.42 (s, 1P). MALDI-HRMS (m/z): calcd 991.2579 ($\text{C}_{54}\text{H}_{54.5}\text{N}_2\text{O}_6\text{P}_2\text{Ru}^+$), found 991.2537.

[(iPr-*p*-C₆H₄-Me)RuCl(Ph₂P-*p*-C₆H₄-CO-Ala-OMe)₂]PF₆, 2_{pA}. Mono complex **1_{pA}** (70 mg, 0.1 mmol), NH_4PF_6 (24.5 mg, 0.15 mmol) and ligand **L_{pA}** (100 mg, 0.25 mmol). Rf (DCM/MeOH 3 %) 0.22. Yield: 84.5 mg (71 %). ^1H NMR (300.13 MHz, CDCl_3) δ /ppm: 7.26–7.58 (m, 28H), 7.03 (d, 2H, $J = 7$ Hz), 5.55 (t, 2H, $J = 4.5$ Hz), 5.24 (d, 1H, $J = 6$ Hz), 5.09 (d, 1H, $J = 6$ Hz), 4.66–4.76 (m, 2H), 3.78 (s, 6H), 2.67–2.76 (m, 1H), 1.54 (d, 6H, $J = 7$ Hz), 1.24 (t, 6H, $J = 7$ Hz), 1.08 (s, 3H). ^{13}C NMR (CDCl_3 , 150.92 MHz) δ /ppm: 15.4 (CH_3 , cymene), 17.9 (C β), 21.54, 21.58 (CHCH_3 , cymene), 31.6 (CHCH_3 , cymene), 49.0 (C α), 52.7 (OMe), 89.3, 89.6 (d, $^2J_{\text{CP}} = 9.5$ Hz, C2, C6, cymene), 97.4, 97.7 (d, $^3J_{\text{CP}} = 3$ Hz, C3, C5, cymene), 101.0 (C4, cymene), 126.9–127.0 (m, C3, phosphine), 128.6–128.8 (m, C3', phosphine), 131.19, 131.22, 131.47 (C4', phosphine), 131.8 (C1, cymene), 133.1–133.9 (m, C1', phosphine), 134.0–134.5 (m, C2, C2', phosphine), 136.3, 136.4 (C4, phosphine), 136.5 (d, $^2J_{\text{CP}} = 43$ Hz, C1, phosphine), 166.58, 166.62 (C(O)NH), 173.4 (COOMe). ^{31}P NMR (CDCl_3 , 242.93 MHz) δ /ppm: –143.96 (septuplet, hexafluorophosphate), 21.26 (d, 1P, $^2J_{\text{PP}} = 52$ Hz), 21.81 (d, 1P, $^2J_{\text{PP}} = 52$ Hz). MALDI-HRMS (m/z): calcd 1019.2892 ($\text{C}_{56}\text{H}_{58}\text{N}_2\text{O}_6\text{P}_2\text{Ru}^+$), found 1019.2852.

[(iPr-*p*-C₆H₄-Me)RuCl(Ph₂P-*m*-C₆H₄-CO-Gly-OMe)₂]PF₆, 2_{mG}. Mono complex **1_{mG}** (80.3 mg, 0.12 mmol), NH_4PF_6 (30.3 mg, 0.19 mmol) and ligand **L_{mG}** (100 mg, 0.26 mmol). Rf (DCM/MeOH 3 %) 0.22. Yield: 46.5 mg (33 %). ^1H NMR (300.13 MHz, CDCl_3) δ /ppm: 7.96 (t, 2H, $J = 5.5$ Hz), 7.78 (d, 2H, $J = 7.5$ Hz), 7.2–7.54 (m, 24H), 7.04 (t, 2H, $J = 5$ Hz), 5.58 (d, 2H, $J = 5.5$ Hz), 5.3 (d, 2H, $J = 6$ Hz), 4.17 (d, 4H, $J = 5.5$ Hz), 3.79 (s, 6H), 2.70–2.80 (m, 1H), 1.23 (d, 6H, $J = 7$ Hz), 1.07 (s, 3H). ^{13}C NMR (CDCl_3 , 150.92 MHz) δ /ppm: 15.4 (CH_3 , cymene), 21.6 (CHCH_3 , cymene), 31.5 (CHCH_3 , cymene), 41.8 (C α), 52.5 (OMe), 89.5 (m, C2, C6, cymene), 97.5 (C4, cymene), 100.9 (C3, C5, cymene), 128.6–128.9 (m, C5, C3', phosphine), 129.6–129.7 (m, C4, phosphine), 131.2, 131.6 (C4', phosphine), 131.4 (C1, cymene), 132.5 (d, $^3J_{\text{CP}} = 7$ Hz, C3, phosphine), 133.5–133.9 (C1, C1', phosphine), 134–134.6 (C2, C2', phosphine), 136.94, 137.0 (d, $^2J_{\text{CP}} = 4$ Hz, C6, phosphine), 166.6, 166.7 (C(O)NH), 170.3 (COOMe). ^{31}P NMR (CDCl_3 , 242.93 MHz) δ /ppm: –143.97 (septuplet, hexafluorophosphate), 21.95 (s, 1P). +ESI MS (m/z): 1025.3 (M^+ , 23 %). MALDI-HRMS (m/z): calcd 991.2579 ($\text{C}_{54}\text{H}_{54}\text{N}_2\text{O}_6\text{P}_2\text{Ru}^+$), found 991.2537.

[(iPr-*p*-C₆H₄-Me)RuCl(Ph₂P-*m*-C₆H₄-CO-Ala-OMe)₂]PF₆, 2_{mA}. Mono complex **1_{mA}** (78.9 mg, 0.11 mmol), NH_4PF_6 (27 mg, 0.17 mmol) and ligand **L_{mA}** (110 mg, 0.28 mmol). Rf (DCM/MeOH 3 %) = 0.26. Yield: 81.2 mg (60 %). ^1H NMR (300.13 MHz, CDCl_3) δ /ppm: 7.92–8.01 (m, 2H), 7.71 (d, 2H, $J = 7.5$ Hz), 7.18–7.56 (m, 24H), 6.81–6.91 (m, 2H), 5.58–5.62 (m, 2H), 5.21–5.30 (m, 4H), 4.62–4.72 (m, 2H), 3.79 (d, 6H, $J = 4$ Hz), 2.69–2.78 (m, 1H), 1.51 (dd, 6H, $J_1 = 7$ Hz, $J_2 = 1$ Hz), 1.21–1.25 (m, 6H), 1.11 (s, 3H). ^{13}C NMR (CDCl_3 ,

75.48 MHz) δ /ppm: 15.5 (CH₃, cymene), 18.17, 18.22 (C β), 21.5, 21.6 (CHCH₃, cymene), 31.5 (CHCH₃, cymene), 48.79, 48.81 (C α), 52.7 (OMe), 89.68, 89.80, 89.85, 89.95 (m, C2, C6, cymene), 97.4, 97.5 (d, $^2J_{CP}$ = 2.5 Hz, C3, C5, cymene), 101.2 (C4, cymene), 128.6, 128.7 (C5, phosphine), 128.9 (d, $^3J_{CP}$ = 16.5 Hz, C3', phosphine), 129.3, 129.5 (C4, phosphine), 131.4, 131.6, 131.7 (C4', phosphine), 131.8 (C1, cymene), 132.3, 132.9 (C1', phosphine), 133.4–133.7 (m, C2, phosphine), 133.8 (C1, phosphine), 134.0 (d, $^3J_{CP}$ = 14.5 Hz, C3', phosphine), 134.4 (C3, phosphine), 134.5–134.8 (m, C2', phosphine), 136.9–137.3 (C6, phosphine), 166.0 (C(O)NH), 173.6, 173.7 (COOMe). ^{31}P NMR (CDCl₃, 242.93 MHz) δ /ppm: -143.84 (septuplet, hexafluorophosphate), 22.08 (d, 1P, $^2J_{PP}$ = 52 Hz), 22.40 (d, 1P, $^2J_{PP}$ = 52 Hz). +ESI MS (m/z): 1053.3 (M⁺, 3 %). MALDI-HRMS (m/z): calcd 1019.2892 (C₅₆H₅₈N₂O₆P₂Ru⁺), found 1019.2852.

[(iPr-*p*C₆H₄-Me)RuCl(Ph₂P-C₂H₄-CO-Gly-OMe)₂]PF₆, **2_{aG}**. Mono complex **1_{aG}** (81.1 mg, 0.13mmol), NH₄PF₆ (32.1 mg, 0.20mmol) and ligand **L_{aG}** (104 mg, 0.32mmol). Rf (DCM/MeOH 5 %) = 0.42. Yield: 60.9 mg (44 %). As mentioned in the discussion, this compound could not be isolated with stratifying purity. ^1H NMR (300.13 MHz, CDCl₃) δ /ppm: 1.22 (d, J = 7 Hz, 6H), 1.84–1.95 (m, 4H), 2.49 (ws, 2H), 2.75 (septuplet, J = 7 Hz, 1H), 3.03–3.15 (m, 2H), 3.72 (s, 3H), 3.91 (d, J = 5.5 Hz, 4H), 5.18 (d, J = 6 Hz, 2H), 5.63–5.67 (m, 2H), 6.06 (t, J = 5 Hz, 2H), 7.36–7.63 (m, 20H). ^{13}C NMR (CDCl₃, 150.92 MHz) δ /ppm: 14.7 (CH₃, cymene), 21.5 (CHCH₃, cymene), 22.3–22.5 (m, C1 phosphine), 31.0 (C2 phosphine), 31.6 (CHCH₃, cymene), 41.4 (C α), 52.4 (OMe), 87.4 (t, $^2J_{CP}$ = 5 Hz, C2, C6, cymene), 97.1 (C4, cymene), 97.7 (C3, C5, cymene), 129.3 (d, $^2J_{CP}$ = 46 Hz, C1', phosphine), 129.30, 129.34, 129.71, 129.75 (d, $^3J_{CP}$ = 5 Hz, C3' phosphine), 131.6, 131.9 (C4, phosphine), 132.16, 132.19, 132.95, 132.98 (d, $^2J_{CP}$ = 4 Hz, C2' phosphine), 132.8 (C1, cymene), 170.3 (COOMe), 171.14, 171.18 (d, $^3J_{CP}$ = 6 Hz, C(O)NH). ^{31}P NMR (CDCl₃, 242.93 MHz) δ /ppm: -143.91 (septuplet, hexafluorophosphate), 20.41 (s, 1P).

[(iPr-*p*C₆H₄-Me)RuCl(Ph₂P-C₂H₄-CO-Ala-OMe)₂]PF₆, **2_{aA}**. Mono complex **1_{aA}** (65.5 mg, 0.10mmol), NH₄PF₆ (24.9 mg, 0.15mmol) and ligand **L_{aA}** (85 mg, 0.25mmol). Rf (DCM/MeOH 5 %) 0.45. Yield: 64.1 mg (42 %). As mentioned in the discussion, this compound could not be isolated with stratifying purity. ^1H NMR (300.13 MHz, CDCl₃) δ /ppm: 1.22 (d, J = 7 Hz, 6H), 1.84–1.95 (m, 4H), 2.49 (ws, 2H), 2.75 (septuplet, J = 7 Hz, 1H), 3.03–3.15 (m, 2H), 3.72 (s, 3H), 3.91 (d, J = 5.5 Hz, 4H), 5.18 (d, J = 6 Hz, 2H), 5.63–5.67 (m, 2H), 6.06 (t, J = 5 Hz, 2H), 7.36–7.63 (m, 20H).

Computational details. All calculations were performed using the Gaussian09 program package (see references section). Geometries were optimized using the wB97xD density functional (Chai and Head-Gordon 2008) in conjunction with the 6-31G(d,p) for the first-row elements and 6-31+G(d,p) basis set for phosphorus and chlorine, while the SDD effective core potential (Andrae et al 1990) was employed for ruthenium. The nature of the stationary points was verified by vibrational analysis at the optimized geometries and no imaginary frequencies were obtained. Total Gibbs energies (G_{tot}) were calculated by summing electronic energies with Gibbs energy correction as obtained from the calculations with default calculation settings and without any scaling of the vibrational frequencies. Visualization of the optimized structures was done by MOLDEN 5.0. (Schafteenaar and Noordik 2000).

Biological testing. All examined organometallic ruthenium complexes were dissolved in DMSO, (c = 10 mM), and stored at -20 °C. Just before use, these stock solutions were diluted with growth medium to the appropriate concentrations; only concentrations of the complexes

below 33.3 μM were used, with the highest DMSO concentration well under 0.5%. Ethacrynic acid (ETA; Sigma-Aldrich, USA), N-Benzyloxycarbonyl-Val-Ala-Asp(O-Me) fluoromethyl ketone (Z-VAD-FMK; Fisher Scientific, USA) and Bafilomycin A1 (BAF A; InvivoGen, USA) were dissolved in DMSO (Sigma-Aldrich) and kept at $-20\text{ }^{\circ}\text{C}$. Caspase 3/7-Glo[®] Assay System (Promega, USA) was dissolved according to producer instruction and kept at $-20\text{ }^{\circ}\text{C}$. Buthionine sulfoximine (BSO; Sigma-Aldrich), N-acetylcysteine (NAC; Sigma-Aldrich) and probenecid were dissolved in water and kept at $-20\text{ }^{\circ}\text{C}$. 3-(4,5-dimethyl-2-thiazolyl)-2,5-diphenyl-2H-tetrazolium bromide (MTT) was purchased by Sigma-Aldrich, dissolved in phosphate-buffered saline and kept by $4\text{ }^{\circ}\text{C}$.

Cell culture. Human cervical carcinoma (HeLa) and laryngeal carcinoma (HEp2) cells were obtained from cell culture bank (GIBCO BRL-Invitrogen, USA). Large cell lung carcinoma (H460) and human breast adenocarcinoma (MDA-MB-213) cells were obtained from American Type Culture Collection (ATCC, USA). Normal human skin keratinocyte were obtained from the foreskin of healthy boys, aged 3–8 years. Foreskin samples were non-inflamed and the children were free of any therapy at least 1 month before the surgery. The cells were obtained at the Neurochemical Laboratory, Department of Chemistry and Biochemistry, School of Medicine, University of Zagreb (Gabrilovac et al 2004). Normal human skin fibroblasts were isolated from the upper arm of a 7-years-old female donor at the Neurochemical Laboratory, Department of Chemistry and Biochemistry, School of Medicine, University of Zagreb. They were used for the cytotoxicity assay at 35 and 40 population doublings. All cell lines were grown as a monolayer culture in Dulbecco's modified Eagle's medium (DMEM; Sigma-Aldrich, USA), supplemented with 10% fetal bovine serum (FBS; Sigma-Aldrich) in a humidified atmosphere of 5% CO_2 at $37\text{ }^{\circ}\text{C}$ and were sub-cultured every 3–4 days.

Cytotoxic assay. Cytotoxic activity of newly synthesized organometallic ruthenium complexes was determined by MTT assay (Mickisch et al 1990) modified accordingly. In short, the cells were seeded into 96-well tissue culture plates. The next day, different concentrations of compounds were added to each well in quadruplicate. Upon 72 h incubation at $37\text{ }^{\circ}\text{C}$, the medium was aspirated, and the MTT dye (Sigma-Aldrich) was added. Three hours later, the formed formazan crystals were dissolved in DMSO, the plates were mechanically agitated for 5 min and the optical density at 545 nm was determined on a microtiter plate reader (Awareness Technology Inc., USA). Sulforhodamine B (SRB; Sigma-Aldrich) was used in order to perform SRB assay according to the protocol (Skehan et al 1990). In short, cultures fixed with trichloroacetic acid were stained for 30 minutes with 0.4% (wt/vol) SRB dissolved in 1% acetic acid. Unbound dye was removed by four washes with 1% acetic acid, and protein-bound dye was extracted with 10 mM unbuffered Tris base [tris (hydroxymethyl)aminomethane] for determination of optical density in a computer-interfaced, 96-well microtiter plate reader (560 nm, Awareness Technology Inc.). The percent of cell survival for each tested concentration of the compounds was calculated according to the absorption value of non-treated control cells, which was set as 100 %.

Potential biomolecular target evaluation. Polynucleotide and protein were purchased as noted: *calf thymus* (ct)-DNA (Sigma) and BSA (bovine serum albumin, Sigma), and dissolved in sodium cacodylate buffer, pH = 7.0, I = 0.05 M. The calf thymus ct-DNA was additionally sonicated and filtered through a 0.45 μm filter (Chaires et al 1982). The ct-DNA concentration was determined spectroscopically at 260 nm using a molar extinction coefficient (ϵ) value of $6550\text{ M}^{-1}\text{ cm}^{-1}$ and it was expressed as the concentration of phosphates (Bresloff and Crothers 1981).

All examined organometallic ruthenium complexes were dissolved in DMSO ($c = 10^{-2}$ M or $c = 10^{-3}$ M), and stored in refrigerator. Stock solutions were diluted with buffer during the experiment or immediately before. The highest DMSO content in solution was $\leq 1\%$. Refrigerated DMSO stock solutions were stable longer than a month, while refrigerated DMSO solutions diluted with buffer were checked to be stable for more than one week. Concentrations of ruthenium complexes below 2×10^{-5} M were used to avoid intermolecular association. At given experimental conditions the absorbance of measured compounds was proportional to their concentrations.

Thermal melting curves for *ct*-DNA and its complexes with studied organometallic ruthenium complexes were determined following the absorption change at 260 nm as a function of temperature (Mergny and Lacroix 2003). Absorbance scale was normalized. T_m values were the midpoints of the transition curves determined from the maximum of the first derivative and checked graphically by the tangent method. The ΔT_m values were calculated by subtracting T_m value of the free polynucleotide from T_m value of the complex. Every ΔT_m value was the average of at least two measurements. The error in ΔT_m is ± 0.5 °C.

CD titrations were performed by adding portions of the compound stock solution into the solution of polynucleotide ($c = 2 \times 10^{-5}$ M) or protein ($c = 2 \times 10^{-6}$ M). Scanning speed was 200 nm min^{-1} , the buffer background was subtracted from each spectrum, while each spectrum was a result of three accumulations.

Fluorimetric titrations were performed by adding aliquots of organometallic ruthenium complexes stock solution into the buffered solution of the BSA protein and by monitoring fluorescence of protein. Excitation wavelength of $\lambda_{\text{exc}} = 300 \text{ nm}$ was used to avoid absorption of excitation light caused by increasing absorbance of the organometallic ruthenium complex. After mixing protein with studied compounds it was observed that equilibrium was reached in less than 120 seconds. Due to low concentrations of studied compounds and protein used in fluorimetric titrations no precipitation occurred. Emission was collected in the range $\lambda_{\text{em}} = 320 - 450 \text{ nm}$. Titration data were processed by non-linear least-square fitting program SPECFIT (Gampp et al 1985, Maeder and Zuberhuhler 1990) that gave the best fit of 1:1 stoichiometry of complexes. The binding constants of complexes of examined compounds with BSA protein were calculated for the concentration range corresponding to ca. 20–80% complexation.

Cell cycle analysis. HeLa cells were seeded into tissue culture plates and treated with either $10 \mu\text{M}$ of **2_{mG}** during 24–72 h or different concentrations of the compound during 72 h, in order to analyze the cell cycle progression. Thereafter, both adherent and floating cells were collected, washed with PBS, fixed in 70% ethanol and left overnight at -20°C . Fixed cells were treated with RNase A (0.1 mg/mL , Sigma-Aldrich) for one hour at room temperature and afterward stained with propidium iodide ($50 \mu\text{g/mL}$, Sigma-Aldrich) for 30 min in the dark. The DNA content was analyzed by flow cytometry NaviosTM (Beckman Coulter, Miami, FL, USA). Data were analyzed with FlowLogic software (Inivai Technologies, Victoria, Australia). Propidium iodide stained samples were analyzed using Watson pragmatic algorithm for modeling cell cycle data.

Cell death analysis. Twenty-four hours after the seeding, HeLa cells were treated either with 10 and $16 \mu\text{M}$ concentrations of **2_{mG}** during 24–72 h or with different concentrations of **2_{mG}** during 72 h. Starved or heat shocked cells were always used as a positive (compensation)

controls. After indicated time point, both adherent and floating cells were collected, centrifuged and washed with PBS. The cell suspension was incubated with Annexin V-FITC (BD Biosciences, USA; according to producer's protocol) and propidium iodide (5 μ g/mL, Sigma-Aldrich). Upon 30 min incubation at room temperature in dark, the viable, early apoptotic, late apoptotic/necrotic and necrotic cell populations were detected and counted by flow cytometry NaviosTM (Beckman Coulter, Miami, FL, USA). Data were analyzed with FlowLogic software (Inivai Technologies, Victoria, Australia).

Twenty-four hours after the seeding, HeLa cells were treated with 22 μ M **2_{mG}**. The total cell lysates were collected 24-72 h upon treatment and loaded onto a 10% SDS polyacrylamide gel and run for two hours at 35 mA. Separated proteins were transferred onto a 0.2 mm nitrocellulose membrane (Schleicher and Schull, Germany) in a Bio-Rad blot cell (Bio-Rad, USA), using buffer consisting of 25 mM Tris/HCl, 86 mM glycine and 20% methanol. To avoid nonspecific binding, the membrane was incubated in blocking buffer (5% non fat dry milk, 0.1% Tween 20 in PBS) for one hour at room temperature and then incubated with anti-PARP (Cell Signaling Technology, USA), Beclin-1 (Santa Cruz Biotechnology, USA) or LCR-I/II antibody (MBL, USA) at room temperature for two hours. After washing the membrane with 0.1% Tween 20 in TBS and incubation with corresponding horseradish peroxidase-coupled secondary antibody (Amersham Pharmacia Biotech, Germany), the proteins were visualized with ECL (Perkin Elmer, USA) according to the manufacturer's protocol. All membranes were incubated with β -Tubulin, which was used as a loading control (Sigma-Aldrich, USA). The role of caspases in **2_{mG}** induced cell death was investigated by MTT assay. HeLa cells were pre-treated for two hours with 6.25 μ M specific pan-caspase inhibitor, Z-VAD. Upon pre-treatment, different concentrations of **2_{mG}** were added and the cytotoxicity effect was determined 72 h later as described above.

The role of autophagy in **2_{mG}** induced cell death was also investigated by MTT assay. HeLa cells were pre-treated for two hours with 0.5 nM specific inhibitor of autophagy, BAF A. Upon pre-treatment, different concentrations of **2_{mG}** were added and the cytotoxicity effect was determined 72 h later as described above.

Determination of glutathione role in cell response. The role of intracellular GSH in cell response to **2_{pG}**, **2_{pA}**, **2_{mG}** and **2_{mA}** was investigated by MTT assay. HeLa cells were either pre-treated overnight with specific inhibitor of GSH synthesis, 0.01 μ g/mL BSO or for two hours with precursor in GSH synthesis, 5 mM NAC. Upon pre-treatment, different concentrations of indicated organometallic complexes were added and the cytotoxicity effect was determined 72 h later as described above. The capacity of GSH to form the detoxification conjugates through enzymatic reaction with **2_{mG}** was investigated by treatment of HeLa cells with combination of 5 or 7.5 μ g/mL ETA (the inhibitor of glutathione S-transferase; the enzyme involved in reaction of GSH with compounds) and different concentrations of **2_{mG}**. The cell survival was examined 72 h after. The optimal concentrations of used modulators of GSH synthesis and glutathione S-transferase reaction were determined previously (Brozovic et al 2008, Brozovic et al 2013, Osmak and Eljuga 1993). The activity of GSH pumps to efflux the GSH-**2_{mG}** conjugates was examined by pre-treatment of HeLa cells for one hour with 0.2 or 0.625 mM probenecid, what was followed by treatment of HeLa cells with different concentrations of **2_{mG}**. Seventy-two hours after, the effect of combination treatment to **2_{mG}** treatment alone was determined.

Determination of total cell ruthenisation. Total cell ruthenisation was measured as described previously for measurement of total cell platination (Brozovic et al 2013) with

modifications. Briefly, the cells were treated with either 150 μM of **2_{pG}**, **2_{pA}**, **2_{mG}** and **2_{mA}** during 2-6 h or 17.5-150 μM **2_{pG}**, **2_{pA}**, **2_{mG}** and **2_{mA}** during 2 h, rinsed with ice-cold PBS, and harvested into 10 ml of ice-cold PBS using a rubber policeman. After centrifugation, the cells were re-suspended in PBS, an aliquot was used for determination of cell number, and the remainder was digested in 70% nitric acid. Cell lysates were heated for 2 h at 75 °C, diluted to 5% nitric acid, and assayed for ruthenium content. The amount of ruthenium was measured by a validated high-resolution inductively coupled plasma mass spectrometry (HR ICPMS) using the Element 2 (Thermo Finnigan, Germany). Calibration standards were prepared from $\text{RuCl}_3 \times 3\text{H}_2\text{O}$ diluted in 1:4 hydrochloric acid and water (1000 $\mu\text{g}/\text{mL}$; Agilent, USA).

Statistical analysis. Data were analyzed by Student's t-test, and expressed as the mean \pm standard error of the mean. Data were considered significant when P values were lower than 0.05, and in the figures these are designated as * = $P < 0.05$ or ** = $P < 0.01$. Experiments were performed in triplicate and repeated at least twice.

Acknowledgement. These materials are based on work financed by the Croatian Science Foundation (CSF, project numbers IP-2014-09-1461, IP-2016-06-1036 and DOK-2018-01-8086), the Terry Fox Foundation, Croatian League Against Cancer and in part by a Croatian-Slovenian bilateral project. The authors would like to thank Professor Maja Osmak and Dr. Mario Cindrić (both Ruđer Bošković Institute) for helpful comments, Ernest Sanders (Ruđer Bošković Institute) for technical assistance and COST Action CM1105 for financial support.

References.

Adhireksan Z, Davey GE, Campomanes P, Groessl M, Clavel CM, Yu HJ *et al* (2014). Ligand substitutions between ruthenium-cymene compounds can control protein versus DNA targeting and anticancer activity. *Nature Communication* **5**: 1-13.

Antonarakis ES, Emadi A (2010). Ruthenium-based chemotherapeutics: are they ready for prime time? *Cancer Chemotherapy and Pharmacology* **66**: 1-9.

Bergamo A, Sava G (2015). Linking the future of anticancer metal-complexes to the therapy of tumour metastases. *Chemical Society Reviews* **44**: 8818-8835.

Biancalana L, Pratesi A, Chiellini F, Zacchini S, Funaioli T, Gabbiani C *et al* (2017). Ruthenium arene complexes with triphenylphosphane ligands: cytotoxicity towards pancreatic cancer cells, interaction with model proteins, and effect of ethacrynic acid substitution. *New Journal of Chemistry* **41**: 14574-14588.

Blunden BM, Rawal A, Lu HX, Stenzel MH (2014). Superior Chemotherapeutic Benefits from the Ruthenium-Based Anti-Metastatic Drug NAMI-A through Conjugation to Polymeric Micelles. *Macromolecules* **47**: 1646-1655.

Bresloff JL, Crothers DM (1981). Equilibrium Studies of Ethidium-Polynucleotide Interactions. *Biochemistry* **20**: 3547-3553.

Brozovic A, Osmak M (2007). Activation of mitogen-activated protein kinases by cisplatin and their role in cisplatin-resistance. *Cancer Letters* **251**: 1-16.

Brozovic A, Majhen D, Roje V, Mikac N, Jakopec S, Fritz G *et al* (2008). $\alpha(v)\beta(3)$ Integrin-mediated drug resistance in human laryngeal carcinoma cells is caused by glutathione-dependent elimination of drug-induced reactive oxidative species. *Molecular Pharmacology* **74**: 298-306.

Brozovic A, Ambriovic-Ristov A, Osmak M (2010). The relationship between cisplatin-induced reactive oxygen species, glutathione, and BCL-2 and resistance to cisplatin. *Critical Reviews in Toxicology* **40**: 347-359.

Brozovic A, Vukovic L, Polancac DS, Arany I, Koberle B, Fritz G *et al* (2013). Endoplasmic reticulum stress is involved in the response of human laryngeal carcinoma cells to Carboplatin but is absent in Carboplatin-resistant cells. *PloS One* **8**: e76397.

Brozovic A, Stojanovic N, Ambriovic-Ristov A, Brozovic Krijan A, Polanc S, Osmak M (2014). 3-Acetyl-bis(2-chloro-4-nitrophenyl)triazene is a potent antitumor agent that induces oxidative stress and independently activates the stress-activated protein kinase/c-Jun NH2-terminal kinase pathway. *Anti-cancer Drugs* **25**: 289-295.

Bugarcic T, Novakova O, Halamikova A, Zerzankova L, Vrana O, Kasparikova J *et al* (2008). Cytotoxicity, cellular uptake, and DNA interactions of new monodentate ruthenium(II) complexes containing terphenyl arenes. *Journal of Medicinal Chemistry* **51**: 5310-5319.

Chaires JB, Dattagupta N, Crothers DM (1982). Studies on Interaction of Anthracycline Antibiotics and Deoxyribonucleic-Acid - Equilibrium Binding-Studies on Interaction of Daunomycin with Deoxyribonucleic-Acid. *Biochemistry* **21**: 3933-3940.

Chaplin AB, Fellay C, Laurency G, Dyson PJ (2007). Mechanistic studies on the formation of $\eta(2)$ -diphosphine ($\eta(6)$ -p-cymene)ruthenium(II) compounds. *Organometallics* **26**: 586-593.

Cimbora-Zovko T, Brozovic A, Piantanida I, Fritz G, Virag A, Alic B *et al* (2011). Synthesis and biological evaluation of 4-nitro-substituted 1,3-diaryltriazenes as a novel class of potent antitumor agents. *European Journal of Medicinal Chemistry* **46**: 2971-2983.

Dikic I, Elazar Z (2018). Mechanism and medical implications of mammalian autophagy. *Nature Reviews Molecular Cell Biology* **19**: 349-364.

Domotor O, Hartinger CG, Bytzek AK, Kiss T, Keppler BK, Enyedy EA (2013). Characterization of the binding sites of the anticancer ruthenium(III) complexes KP1019 and

KP1339 on human serum albumin via competition studies. *Journal of biological inorganic chemistry* **18**: 9-17.

Dos Santos ER, Correa RS, Ribeiro JU, Graminha AE, Ellena J, Selistre-de-Araujo HS *et al* (2016). Ru(II)/bisphosphine/diimine/amino acid complexes: diastereoisomerism, cytotoxicity, and inhibition of tumor cell adhesion to collagen type I. *Journal of Coordination Chemistry* **69**: 3518-3530.

Fischer U, Janicke RU, Schulze-Osthoff K (2003). Many cuts to ruin: a comprehensive update of caspase substrates. *Cell Death and Differentiation* **10**: 76-100.

Gabrilovac J, Cupic B, Breljak D, Zekusic M, Boranic M (2004). Expression of CD13/aminopeptidase N and CD10/neutral endopeptidase on cultured human keratinocytes. *Immunology Letters* **91**: 39-47.

Galluzzi L, Senovilla L, Vitale I, Michels J, Martins I, Kepp O *et al* (2012). Molecular mechanisms of cisplatin resistance. *Oncogene* **31**: 1869-1883.

Gampp H, Maeder M, Meyer CJ, Zuberbuhler AD (1985). Calculation of Equilibrium-Constants from Multiwavelength Spectroscopic Data .2. Specfit - 2 User-Friendly Programs in Basic and Standard Fortran-77. *Talanta* **32**: 257-264.

Gasser G, Ott I, Metzler-Nolte N (2011). Organometallic Anticancer Compounds. *Journal of Medicinal Chemistry* **54**: 3-25.

Gaussian 09, Revision E.01, Frisch MJ, Trucks GW, Schlegel HB, Scuseria GE, Robb MA, Cheeseman JR *et al*, Gaussian, Inc., Wallingford CT, 2009.

Gridnev ID, Imamoto T (2015). Challenging the Major/Minor Concept in Rh-Catalyzed Asymmetric Hydrogenation. *ACS Catalysis* **5**: 2911-2915.

Kaufmann SH, Desnoyers S, Ottaviano Y, Davidson NE, Poirier GG (1993). Specific proteolytic cleavage of poly(ADP-ribose) polymerase: an early marker of chemotherapy-induced apoptosis. *Cancer Research* **53**: 3976-3985.

Kirin SI, Schatzschneider U, de Hatten X, Weyhermuller T, Metzler-Nolte N (2006). 1,n '-disubstituted ferrocenoyl amino acids and dipeptides: Conformational analysis by CD spectroscopy, X-ray crystallography, and DFT calculations. *Journal of Organometallic Chemistry* **691**: 3451-3457.

Klionsky DJ, Abdalla FC, Abeliovich H, Abraham RT, Acevedo-Arozena A, Adeli K *et al* (2012). Guidelines for the use and interpretation of assays for monitoring autophagy. *Autophagy* **8**: 445-544.

Kokan Z, Kirin SI (2012). The application of "backdoor induction" in bioinspired asymmetric catalysis. *RSC Advances* **2**: 5729-5737.

Kokan Z, Kirin SI (2013). "Backdoor Induction" of Chirality in Asymmetric Hydrogenation with Rhodium(I) Complexes of Amino Acid Substituted Triphenylphosphane Ligands. *European Journal of Organic Chemistry* **2013**: 8154-8161.

Kokan Z, Glasovac Z, Elenkov MM, Gredicak M, Jeric I, Kirin SI (2014). "Backdoor Induction" of Chirality: Asymmetric Hydrogenation with Rhodium(I) Complexes of Triphenylphosphane-Substituted beta-Turn Mimetics. *Organometallics* **33**: 4005-4015.

Kokan Z, Peric B, Kovacevic G, Brozovic A, Metzler-Nolte N, Kirin SI (2017). cis-versus trans-Square-Planar Palladium(II) and Platinum(II) Complexes with Triphenylphosphine Amino Acid Bioconjugates. *European Journal of Inorganic Chemistry*: 3928-3937.

Kokan Z, Kovacevic B, Stefanic Z, Tzvetkova P, Kirin SI (2018). Controlling orthogonal self-assembly through cis-trans isomerization of a non-covalent palladium complex dimer. *Chemical Communication* **54**: 2094-2097.

Komor AC, Barton JK (2013). The path for metal complexes to a DNA target. *Chemical Communication* **49**: 3617-3630.

Levine B, Kroemer G (2008). Autophagy in the pathogenesis of disease. *Cell* **132**: 27-42.

Li J, Yuan J (2008). Caspases in apoptosis and beyond. *Oncogene* **27**: 6194-6206.

Lin Y, Huang Y, Zheng W, Wang F, Habtemariam A, Luo Q *et al* (2013). Organometallic ruthenium anticancer complexes inhibit human glutathione-S-transferase pi. *Journal of Inorganic Biochemistry* **128**: 77-84.

Liu CY, Takemasa A, Liles WC, Goodman DB, Jonas M, Rosen H, *et al* (2003). Broad-spectrum caspase inhibition paradox-ically augmented cell death in TNF α -stimulated neutrophils. *Blood* **101**: 295-304.

Liu Z, Habtemariam A, Pizarro AM, Fletcher SA, Kisova A, Vrana O *et al* (2011). Organometallic half-sandwich iridium anticancer complexes. *Journal of Medicinal Chemistry* **54**: 3011-3026.

Maeder M, Zuberbuhler AD (1990). Nonlinear Least-Squares Fitting of Multivariate Absorption Data. *Analytical Chemistry* **62**: 2220-2224.

Martinez MA, Carranza MP, Massaguer A, Santos L, Organero JA, Aliende C *et al* (2017). Synthesis and Biological Evaluation of Ru(II) and Pt(II) Complexes Bearing Carboxyl Groups as Potential Anticancer Targeted Drugs. *Inorganic Chemistry* **56**: 13679-13696.

Meier-Menches SM, Gerner C, Berger W, Hartinger CG, Keppler BK (2018). Structure-activity relationships for ruthenium and osmium anticancer agents - towards clinical development. *Chemical Society Reviews* **47**: 909-928.

Mergny JL, Lacroix L (2003). Analysis of thermal melting curves. *Oligonucleotides* **13**: 515-537.

Mickisch G, Fajta S, Keilhauer G, Schlick E, Tschada R, Alken P (1990). Chemosensitivity testing of primary human renal cell carcinoma by a tetrazolium based microculture assay (MTT). *Urological Research* **18**: 131-136.

Millan G, Gimenez N, Lara R, Berenguer JR, Moreno MT, Lalinde E *et al* (2019). Luminescent Cycloplatinated Complexes with Biologically Relevant Phosphine Ligands: Optical and Cytotoxic Properties. *Inorganic Chemistry* **58**: 1657-1673.

Minenkov Y, Singstad A, Occhipinti G, Jensen VR (2012). The accuracy of DFT-optimized geometries of functional transition metal compounds: a validation study of catalysts for olefin metathesis and other reactions in the homogeneous phase. *Dalton Transactions* **41**: 5526-5541.

Nikoletopoulou V, Markaki M, Palikaras K, Tavernarakis N (2013). Crosstalk between apoptosis, necrosis and autophagy. *Biochimica et Biophysica Acta* **1833**: 3448-3459.

Novakova O, Kasparkova J, Bursova V, Hofr C, Vojtiskova M, Chen HM *et al* (2005). Conformation of DNA modified by monofunctional Ru(II) arene complexes: Recognition by DNA binding proteins and repair. Relationship to cytotoxicity. *Chemistry & Biology* **12**: 121-129.

Opačak S., Kokan Z., Glasovac Z., Perić B., Kirin, S. I. (2019) "Backdoor induction" of chirality: Trans-1,2-cyclohexanediamine as key building block for asymmetric hydrogenation catalysts, *European Journal Organic Chemistry*, in press, doi: 10.1002/ejoc.201801647.

Osmak M, Eljuga D (1993). The characterization of two human cervical carcinoma HeLa sublines resistant to cisplatin. *Research in Experimental Medicine* **193**: 389-396.

Osmak M, Brozovic A, Ambriovic-Ristov A, Hadzija M, Pivcevic B, Smital T (1998). Inhibition of apoptosis is the cause of resistance to doxorubicin in human breast adenocarcinoma cells. *Neoplasma* **45**: 223-230.

Otagiri M, Giam Chuang VS (Eds.), (2016) *Albumin in Medicine. Pathological and Clinical Applications*, Springer. ISBN 978-981-10-2116-9

Pongratz M, Schluga P, Jakupec MA, Arion VB, Hartinger CG, Allmaier G *et al* (2004). Transferrin binding and transferrin-mediated cellular uptake of the ruthenium coordination compound KP1019, studied by means of AAS, ESI-MS and CD spectroscopy. *Journal of Analytical Atomic Spectrometry* **19**: 46-51.

Puckett CA, Ernst RJ, Barton JK (2010). Exploring the cellular accumulation of metal complexes. *Dalton Transactions* **39**: 1159-1170.

Qi SC, Hayashi J, Zhang L (2016). Recent application of calculations of metal complexes based on density functional theory. *RSC Advances* **6**: 77375-77395.

Rathgeb A, Bohm A, Novak MS, Gavriluta A, Domotor O, Tornmasino JB *et al* (2014). Ruthenium-Nitrosyl Complexes with Glycine, L-Alanine, L-Valine, L-Proline, D-Proline, L-Serine, L-Threonine, and L-Tyrosine: Synthesis, X-ray Diffraction Structures, Spectroscopic and Electrochemical Properties, and Antiproliferative Activity. *Inorganic Chemistry* **53**: 2718-2729.

Ravera M, Baracco S, Cassino C, Colangelo D, Bagni G, Sava G *et al* (2004). Electrochemical measurements confirm the preferential bonding of the antimetastatic complex [ImH][RuCl₄(DSMO)(Im)] (NAMI-A) with the proteins and the weak interaction with nucleobases. *Journal of Inorganic Biochemistry* **98**: 984-990.

Peters T, Jr., (1995) All About Albumin. Biochemistry, Genetics, and Medical Applications, Elsevier Inc. ISBN: 978-0-12-552110-9

Saez R, Lorenzo J, Prieto MJ, Font-Bardia M, Calvet T, Onnenaca N *et al* (2014). Influence of PPh₃ moiety in the anticancer activity of new organometallic ruthenium complexes. *Journal of Inorganic Biochemistry* **136**: 1-12.

Sava G, Frausin F, Cocchietto M, Vita F, Podda E, Spessotto P *et al* (2004). Actin-dependent tumour cell adhesion after short-term exposure to the antimetastasis ruthenium complex NAMI-A. *European Journal of Cancer* **40**: 1383-1396.

Schaftenaar G, Noordik JH (2000). Molden: a pre- and post-processing program for molecular and electronic structures. *Journal of Computer-Aided Molecular Design* **14**: 123-134.

Scolaro C, Chaplin AB, Hartinger CG, Bergamo A, Cocchietto M, Keppler BK *et al* (2007). Tuning the hydrophobicity of ruthenium(II)-arene (RAPTA) drugs to modify uptake, biomolecular interactions and efficacy. *Dalton Transactions*: 5065-5072.

Scrase TG, O'Neill MJ, Peel AJ, Senior PW, Matthews PD, Shi H *et al* (2015). Selective lability of ruthenium(II) arene amino acid complexes. *Inorganic Chemistry* **54**: 3118-3124.

Sersen S, Kljun J, Kryeziu K, Panchuk R, Alte B, Korner W *et al* (2015). Structure-Related Mode-of-Action Differences of Anticancer Organoruthenium Complexes with beta-Diketonates. *Journal of Medicinal Chemistry* **58**: 3984-3996.

Skehan P, Storeng R, Scudiero D, Monks A, McMahon J, Vistica D *et al* (1990). New colorimetric cytotoxicity assay for anticancer-drug screening. *Journal of National Cancer Institute* **82**: 1107-1112.

Sommer MG, Kureljak P, Urankar D, Schweinfurth D, Stojanovic N, Bubrin M *et al* (2014). Combining [Arene-Ru] with Azocarboxamide to Generate a Complex with Cytotoxic Properties. *Chemistry-a European Journal* **20**: 17296-17299.

Stojanovic N, Urankar D, Brozovic A, Ambriovic-Ristov A, Osmak M, Kosmrlj J (2013). Design and evaluation of biological activity of diazenecarboxamide-extended cisplatin and carboplatin analogues. *Acta Chimica Slovenica* **60**: 368-374.

Tewari M, Quan LT, O'Rourke K, Desnoyers S, Zeng Z, Beidler DR *et al* (1995). Yama/CPP32 beta, a mammalian homolog of CED-3, is a CrmA-inhibitable protease that cleaves the death substrate poly(ADP-ribose) polymerase. *Cell* **81**: 801-809.

Townsend DM, Tew KD (2003). The role of glutathione-S-transferase in anti-cancer drug resistance. *Oncogene* **22**: 7369-7375.

Vajs J, Steiner I, Brozovic A, Pevec A, Ambriovic-Ristov A, Matkovic M *et al* (2015). The 1,3-diaryltriazenido(p-cymene)ruthenium(II) complexes with a high in vitro anticancer activity. *Journal of Inorganic Biochemistry* **153**: 42-48.

Vandenabeele P, Grootjans S, Callewaert N, Takahashi N (2013). Necrostatin-1 blocks both RIPK1 and IDO: consequences for the study of cell death in experimental disease models. *Cell Death and Differentiation* **20**: 185-187.

Wang FY, Xu JJ, Habtemariam A, Bella J, Sadler PJ (2005). Competition between glutathione and guanine for a ruthenium(II) arene anticancer complex: Detection of a sulfenato intermediate. *Journal of the American Chemical Society* **127**: 17734-17743.

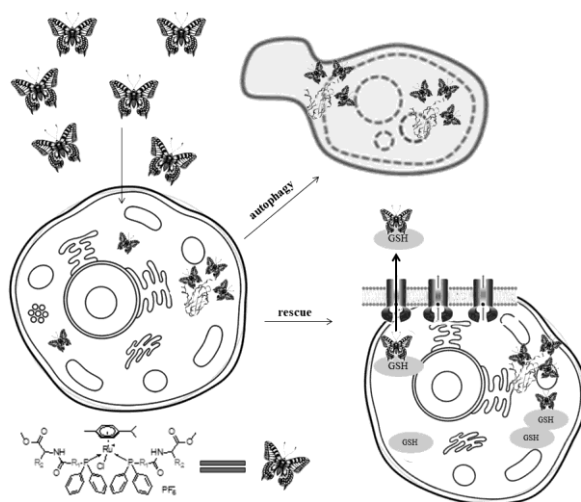
Wu Y-T, Tan H-L, Shui G, Bauvy C, Huang Q, Wenk MR *et al* (2010). Dual role of 3-methyladenine in modulation of autophagy via different temporal patterns of inhibition on class I and III phosphoinositide 3-kinase. *The Journal of Biological Chemistry* **285**: 10850-10861.

Zaman GJ, Lankelma J, van Tellingen O, Beijnen J, Dekker H, Paulusma C *et al* (1995). Role of glutathione in the export of compounds from cells by the multidrug-resistance-associated

protein. *Proceedings of the National Academy of Sciences of the United States of America* **92**:
7690-7694.

ACCEPTED MANUSCRIPT

Graphical abstract.



Highlights.

A set of (*p*-cymene)-ruthenium amino acid bioconjugates **1** and **2** is reported.

The bioconjugates **2** show micromolar affinity for proteins.

Increased potency and selectivity of **2** towards cancer cell lines is detected.

The cytotoxicity of bioconjugates **2** is in correlation with their BSA binding constants.

Cell stress response includes increase of cells in S phase of cell cycle, induction of autophagy and use of GSH as detoxification mechanism.